NAVAL POSTGRADUATE SCHOOL

MONTEREY, CALIFORNIA

THESIS

DETERMINATION OF YOUNG'S MODULUS OF CARBON NANOTUBES USING MD SIMULATION

by

Oh, Jung Joo

December 2003

Thesis Co-Advisors: Young W. Kwon
James H. Luscombe

Approved for public release; distribution is unlimited.

THIS PAGE INTENTIONALLY LEFT BLANK

REPORT DOCUMENTATION PAGE			Form Approved OMB No. 0704-0188
Public reporting burden for this collection of information is estimated to average 1 hour per response, including the time for reviewing instruction, searching existing data sources, gathering and maintaining the data needed, and completing and reviewing the collection of information. Send comments regarding this burden estimate or any other aspect of this collection of information, including suggestions for reducing this burden, to Washington headquarters Services, Directorate for Information Operations and Reports, 1215 Jefferson Davis Highway, Suite 1204, Arlington, VA 22202-4302, and to the Office of Management and Budget, Paperwork Reduction Project (0704-0188) Washington DC 20503.			
1. AGENCY USE ONLY ***(Leave blank)***	**2. REPORT DATE** December 2003	**3. REPORT TYPE AND DATES COVERED** Master's Thesis	
4. TITLE AND SUBTITLE: Determination of Young's Modulus of Carbon Nanotube Using Molecular Dynamics (MDSS) Simulation			**5. FUNDING NUMBERS**
6. AUTHOR(S) Oh, Jung Joo			
7. PERFORMING ORGANIZATION NAME(S) AND ADDRESS(ES) Naval Postgraduate School Monterey, CA 93943-5000			**8. PERFORMING ORGANIZATION REPORT NUMBER**
9. SPONSORING /MONITORING AGENCY NAME(S) AND ADDRESS(ES) N/A			**10. SPONSORING/MONITORING AGENCY REPORT NUMBER**
11. SUPPLEMENTARY NOTES The views expressed in this thesis are those of the author and do not reflect the official policy or position of the Department of Defense or the U.S. Government.			
12a. DISTRIBUTION / AVAILABILITY STATEMENT Approved for public release; distribution is unlimited			**12b. DISTRIBUTION CODE**

13. ABSTRACT (maximum 200 words)

Molecular dynamics simulations were performed to determine the Young's modulus of the single-walled carbon nanotubes (SWNT) and bamboo structural carbon nanoutbes (BSNT) models generated from the basic structure characteristics of graphite. The empirical Tersoff-Brenner potential and freestanding thermal vibration methods proposed by Krishnan et al. were used to determine the interatomic forces and *rms* displacements of carbon atoms at room temperature ~300 K. The calculated average Young's modulus of SWNT and BSNT model were <Y> = 1.424 and 0.604 TPa, respectively. In particular, the calculated Y value of the SWNT model is in good agreement with the previous measurements. Although, the evaluated Y value of the BSNT model, which represents heterogeneous nanotubes, was less than the pure the SWNT model, it still has strong and stiff mechanical properties comparing with other general bulk materials such as hardened steel (210 GPa). CNTs hold a promising future for the variety of potential applications in the nanotechnology field.

14. SUBJECT TERMS Molecular Dynamics, MDSS, Carbon Nanotubes, SWNT, BSWNT, Young's Modulus, Equilibrium Analysis, Non-Equilibrium Analysis, CNT, Tersoff-Brenner Potential			**15. NUMBER OF PAGES** 75
			16. PRICE CODE
17. SECURITY CLASSIFICATION OF REPORT Unclassified	**18. SECURITY CLASSIFICATION OF THIS PAGE** Unclassified	**19. SECURITY CLASSIFICATION OF ABSTRACT** Unclassified	**20. LIMITATION OF ABSTRACT** UL

NSN 7540-01-280-5500 Standard Form 298 (Rev. 2-89)
Prescribed by ANSI Std. 239-18

THIS PAGE INTENTIONALLY LEFT BLANK

Approved for public release; distribution is unlimited

DETERMINATION OF YOUNG'S MODULUS OF CARBON NANOTUBES USING MOLECULAR DYNAMICS (MDSS) SIMULATION

Oh, Jung Joo
Major, Korean Army
B. S., Korea Military Academy, 1991

Submitted in partial fulfillment of the
requirements for the degree of

MASTER OF SCIENCE IN APPLIED PHYSICS

from the

NAVAL POSTGRADUATE SCHOOL
December 2003

Author: Oh, Jung Joo

Approved by: Young W. Kwon
Thesis Co-Advisor

James H. Luscombe
Thesis Co-Advisor

James H. Luscombe
Chairman, Department of Physics

THIS PAGE INTENTIONALLY LEFT BLANK

ABSTRACT

Molecular dynamics simulations were performed to determine the Young's modulus of the single-walled carbon nanotubes (SWNT) and bamboo structural carbon nanoutbes (BSNT) models generated from the basic structure characteristics of graphite. The empirical Tersoff-Brenner potential and freestanding thermal vibration methods proposed by Krishnan et al. were used to determine interatomic forces and *rms* displacements of carbon atoms at room temperature ~300 K. The calculated average Young's modulus of SWNT and BSNT model were <Y> = 1.424 and 0.604 TPa, respectively. In particular, the calculated Y value of the SWNT model is in good agreement with the previous measurements. Although, the evaluated Y value of the BSNT model, which represents heterogeneous nanotubes, was less than the pure the SWNT model, it still has strong and stiff mechanical properties comparing with other general bulk materials such as hardened steel (210 GPa). CNTs hold a promising future for the variety of potential applications in the nanotechnology field.

THIS PAGE INTENTIONALLY LEFT BLANK

TABLE OF CONTENTS

THIS PAGE INTENTIONALLY LEFT BLANK

LIST OF FIGURES

THIS PAGE INTENTIONALLY LEFT BLANK

LIST OF TABLES

THIS PAGE INTENTIONALLY LEFT BLANK

ACKNOWLEDGMENTS

I sincerely thank the following people who assisted me to in completing this thesis: Prof. Kwon provided the modified MDSS simulation source code, which was the main source to investigate the mechanical properties of Carbon Nanotubes, and clear guidance, kept the project on track, and ensured the quality of the final product. Prof. Luscombe instructed me on physics from the introductory mechanics to the quantum mechanics, since I arrived at NPS. Most of the physical and mechanical inspirations on my thesis could not be obtained without Prof. Luscombe's instructions.

Also, I would like to thank the Republic of Korea Army (ROKA) and Korea Defense Security Command (DSC). Both institutions provided me with the opportunities to study advanced educational materials and gave moral support to complete my thesis work.

Finally, I would like to give gratitude to my mother, wife and children, Hyun su-jin, Ha-rim and June-suk. Although they could not stay with me in Monterey, CA, they always encouraged me to focus on this study. I admire their patience and understanding during the last two years.

THIS PAGE INTENTIONALLY LEFT BLANK

I. INTRODUCTION

A. BACKGROUND

Since their discovery by Iijima in 1991, carbon nanotubes (CNTs), which are formed of seamless cylindrical graphite layers and known as perfect structural materials, have been the subject of numerous experimental and molecular dynamics (MD) simulations in the nanotechnology field because of their superior mechanical and electronic properties [1]. In particular, the high Young's modulus and other excellent mechanical properties of CNTs guarantee a great future potential for extremely strong light-weight composite materials in structural applications such as body armor, polymer matrix composites, and reinforcement material.

The Young's modulus of a material is a unique mechanical property that directly reflects the binding force among constituent atoms. The greater Young's modulus is, the larger is the force required for the same amount of elastic deformation of the given material. If a material were composed of an imperfect bonding network between atoms, its Young's modulus would become lower than a material with a perfect internal structure. Thus, many researchers have focused on new materials with a high Young's modulus and a perfect bonding-network to strengthen composite structures.

For that purpose, carbon fibers have already been used to reinforce other materials for many years because of their low density and high tensile strength (2~5 GPa for fibers [2,3] and up to 20 GPa for 'whiskers' [4], as compared to 1~2 GPa for most high-strength steels). Now, however, CNTs become a matter of primary concern to replace carbon fibers, because typical carbon fibers contain many structural defects and have a lower effective Young's modulus than CNTs.

So far, there have been many theoretical and experimental results suggesting that the Young's modulus of CNTs may be slightly larger than that for planar graphite of 1.02 TPa [5] and that for diamond crystal of 0.827 TPa [6], both of which are made of a covalently bonded network of carbon atoms. Recently, with the advance of

nanotechnology, the study of CNTs embedded within a polymer or metal matrix has leaped into prominence in the nanotechnology field. Thus, the accurate evaluation of Young's modulus of nanotubes is an important first step in developing composite materials so that their extraordinary high strength and stiffness can be realized in the near future.

However, although theoretical calculations have predicted a wide range of Young's moduli for CNTs as 0.8 ~5.5 TPa [7~9], there are disputes to accepting an effective Young's modulus for CNT's because predicting mechanical properties of macroscopic systems from the microscopic nature of their constituent atoms is a difficult problem. Conventionally, direct measurements for the elastic modulus of bulk materials can be evaluated under tensile or compressive loading tests, but for carbon nanotubes this has proved challenging due to their extremely small size; they are about 10 nm or less in diameter and about 10,000 times smaller than a human hair. So, they cannot be manipulated and measured as easily without special treatments.

Consequently, unlike other fields in science and engineering, computational nanotechnology using modeling and simulation techniques connected with continuum mechanics, quantum mechanics and molecular dynamics has played a major role in predicting as well as explaining the interesting mechanical properties of various CNTs. To complement the weak points in the current computational techniques, in general, the electronic optics devices such as transmission electron microscopes (TEM), atomic force microscopy (AFM) and scanning electron microscopy (SEM) may be useful in that field.

Recently, scientists have published some interesting results in the field of nanoscale devices and composite materials; they have found that controlling or shaping nanotube geometries is important for many future applications. One such possibility is to connect nanotubes of different diameters through topological defect mediated junctions [10] and simply forming physically contacted or touching junctions as shown in Figure 1(a) [11]. Figure 1(a) demonstrates four kinds of possible "Y" junctions in which the chirality and tube diameter of the branches differ from that of their stems, and the atoms

forming defect rings are shown in dark. These special defect configurations will play an important roll in modeling of heterogeneous carbon nanotubes, and will be described in detail later.

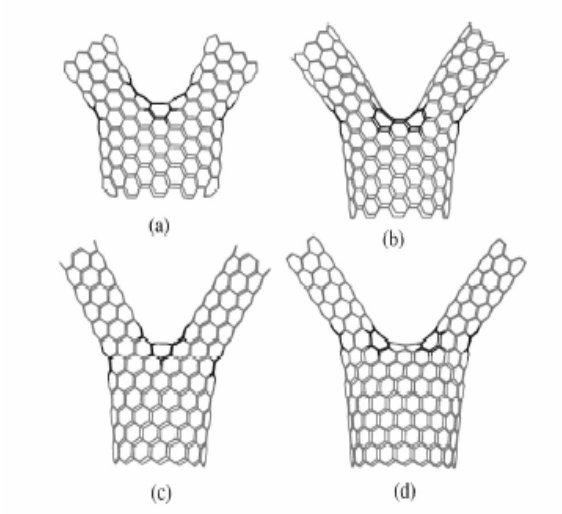

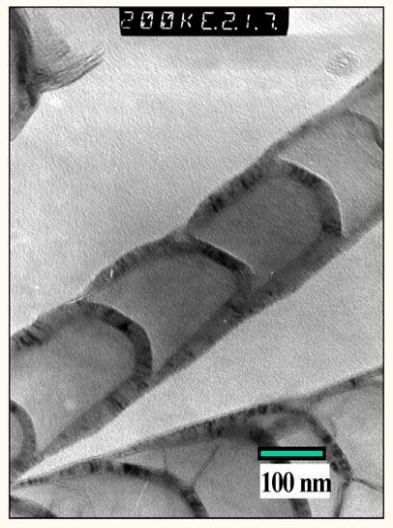

(a) Four possible Y-junction (b) TEM Image BSNT

Figure 1. Four possible Y-junctions [12] and TEM Image of BSNT [13]

Meanwhile, according to the Korea Iljin-Nanotech R&D Center, bamboo structural carbon nanotubes (BSNT) that have internal half-dome shaped membrane structures between multi-wall carbon nanotube (MWNT) side walls and look like a so-called "bamboo node" that is the rigid membrane between hollow segments of real bamboo stems, can be synthesized by the chemical vapor deposition (CVD) growth method, and are shown in Figure 1(b) [13]. Figure 1(b) shows that the spacing of joints in the BSNT has certain regularity and that the internal diameter can be varied as the bamboo structure forms with the external diameter not changed.

The above theoretical studies and observations provide feasible possibilities that various hetero-junction structures of CNT's can be synthesized to build up numerous nano-scale devices, as well as be used for the embedded CNTs composite materials. Thus, we have to pay attention to how such hetero-junction structures of nanotubes will

affect the changes of Young's modulus and deformation behaviors of CNT's systems by using molecular dynamics (MD) simulation.

In recent years, numerical simulations of finite systems have become more common due to the availability of powerful computers. Therefore, various MD simulation codes have been developed, such as Car-Parrinello (CP) code using the ab-initio quantum density functional method, tight-binding molecular dynamics (TBMD) code, and classical MD code. In computational nanotechnology research, these three type simulation methods can be used in a complimentary fashion to improve computational accuracy and efficiency [14].

However, as previously mentioned, computing the Young's modulus of CNT's and predicting mechanical deformation behaviors from the MD simulations is not an easy task. In particular, although the more accurate ab-initio MD code based on quantum mechanics is known as the best way to extract nano-scale physical properties of CNT's, its application on desktop computers may be a time consuming process due to the relatively high computational costs resulting from many-body interactions connected with electronic phenomena. Instead, the use of the classical MD simulation method, which adopts a realistic empirical many-body potential function and treats atoms or molecules as classical particles, would be well justified except when chemical changes involving electronic rearrangements with large atomic displacements are expected to occur [15].

B. OBJECTIVES

In this thesis, we will explore the use of a combination of the classical MD simulation method and the atomic thermal vibration analysis to model the single-walled nanotubes (SWNT) and hetero-junction CNTs such as BSNT, for the purpose of calculating the Young's modulus for both models, and to investigate the mechanical deformation behaviors in both models.

To do that, the basic structural characteristics of CNTs will be presented in order to model initial geometries of SWNT and BSNT as a first step. Then, the classical MD simulation theory used for the equilibrium and non-equilibrium dynamic analysis will be discussed with the introduction of the Tersoff-Brenner (T-B) type potential, which is well parameterized and particularly suited for SWNT and BSNT.

Furthermore, the methodology of the freestanding room temperature CNT vibration analysis based on the continuum and quantum mechanics will be described and applied to the evaluation of Young's modulus of SWNT and BSNT with statistical approaches from the carbon atom trajectory data in MD simulation. This method was based on the stochastically driven oscillator analysis, in which Krishnan *et al*. showed that the Young's modulus of nanotubes could be inferred by measuring the thermal vibration amplitude of freestanding nanotube end-tips in the TEM [16]. As a final step, an estimation of the validity of the classical MD and thermal vibration methods applied in this thesis will be made by introducing a comparative analysis of whether the evaluated Young's moduli of SWNT and BSNT from classical MD simulation results are reasonable and comparable with each other.

THIS PAGE INTENTIONALLY LEFT BLANK

II. MODELING, RELATED THEORY, AND METHODOLOGY

This chapter describes the basic structure of carbon nanotubes necessary for modeling initial geometries of SWNT and BSNT, the classical MD simulation theory with the empirical Tersoff-Brenner potential function, and the methodology of determining Young's modulus from the MD simulation using the thermal vibration analysis method presented by Krishnan et al.

A. MODELING OF SWNT AND BSNT FROM BASIC STRUCTURES

Understanding the basic geometrical structures of carbon nanotubes is a preliminary essential step to start MD simulations with the initial geometrical configurations of the given CNT's systems. For example, it should be a properly energy-minimized structure. This section describes the basic structural properties of carbon nanotubes, explains the synthesis possibility of the hetero-junction type nanotubes such as the BSNT, and then presents the resultant initial geometrical models of SWNT and BSWNT before operating the MD simulations.

1. Basic Structures of Nanotubes

Many experiments have confirmed that carbon nanotubes are cylindrical tubular shell structures based on a benzene-type hexagonal lattice of carbon atoms. The cylindrical tube can be tens of microns long, and the ends of nanotubes are "capped" with half-dome shaped fullerene molecules.

The ideal single-walled carbon nanotube (SWNT) can be thought of as the fundamental structure, which form the building blocks of both multi-walled carbon nanotubes (MWNT) and ordered array of SWNT's called nanoropes. It is known that the Young's modulus of MWNT is not significantly different from SWNT, because the high modulus mainly results from the carbon-carbon interaction bonds within the individual layers. In addition, there is only a weak Van der Waals interaction force between two graphite layers because the average inter-layer spacing distance of 3.4 Å is larger than the maximum carbon-carbon bond length of ~2.0 Å. Thus, once understanding of the SWNT

structures is obtained, the consideration of other structures of CNTs is much easier. Consequently, the outline for the basic structural characteristics of CNTs will focus on the SWNT [17].

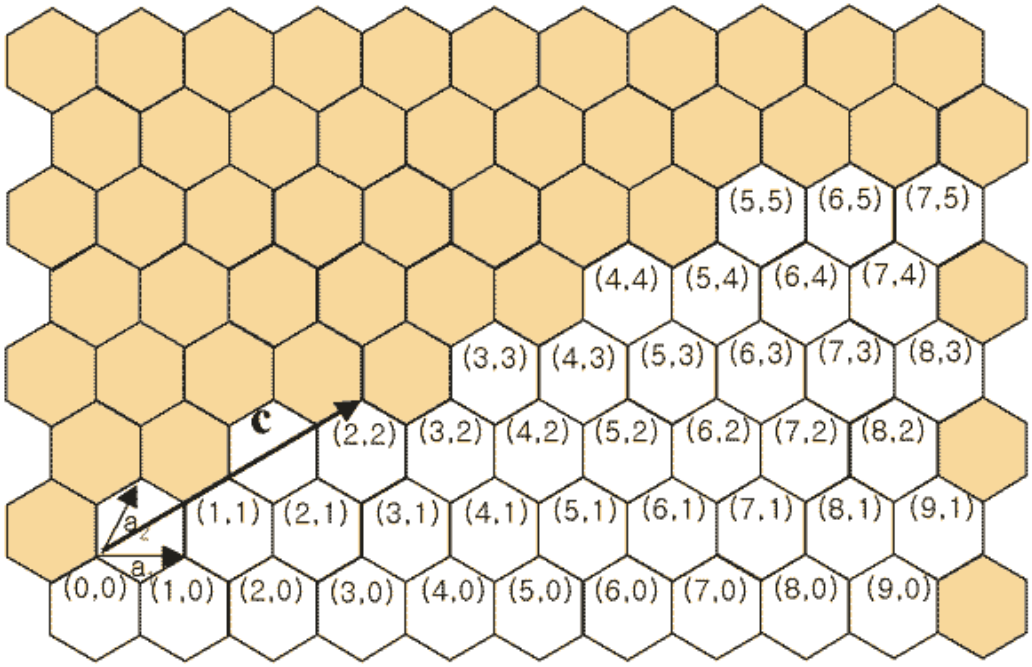

Figure 2. Graphite layer with carbon atoms labeled using (n, m) notation [13].

To date, it has been found that three types of CNTs are possible, called armchair, zigzag and chiral SWNT, which depend on how the two-dimensional graphite layer is rolled up. To understand the structural features of SWNT, Figure 2 shows the two-dimensional graphite layer with atoms labeled using (n, m) notation, where n and m are integers and typically n $\geq$ m; this notation was suggested by Dresselhaus *et al*. [18]. In Figure 2, the vector $\vec{C}$ is called the chiral vector of the nanotube, and is defined as $\vec{C} = n\vec{a}_1 + m\vec{a}_2$, where $\vec{a}_1$ and $\vec{a}_2$ are unit vectors in the two-dimensional hexagonal graphite sheet. The magnitude of these unit vectors is known to be 0.246 nm.

The physical properties of carbon nanotubes are significantly determined by their diameter and chiral angle, both of which depend on n and m. When the graphite layer is rolled up to form the cylindrical part of the nanotubes, the ends of the chiral vector meet each other. Thus, the chiral vector forms the circumference of the nanotube's circular cross-section, and different values of n and m, therefore, lead to different natotube structures. The diameter of nanotubes, d_t, is simply the length of the chiral vector divided by π, and thus it can be expressed as a function of n and m,

$$d_t = \frac{0.246}{\pi}(n^2 + n \cdot m + m^2)^{1/2} \text{ (nm)} \qquad (1)$$

The chiral angle, which is the angle between $\vec{C}$ and $\vec{a}_1$ as shown in Figure 2, can be calculated by,

$$\theta = \sin^{-1}\left\{\frac{3^{1/2} \cdot m}{2(n^2 + n \cdot m + m^2)^{1/2}}\right\} \qquad (2)$$

According to prior research, armchair nanotubes are formed when n = m and the chiral angle is 30°. Zigzag nanotubes are formed when either n or m are zero with the chiral angle 0°. All other nanotubes are known as chiral nanotubes with the chiral angle is between 0~30° [19]. In particular, the chiral vector (n, m) can determine whether a SWNT can be either a metal or semiconductor. For example, a metallic nanotube can be obtained when the difference n-m is a multiple of three. If the difference is not a multiple of three, a semiconductor nanotube can be obtained. These characteristics are very important to study the electronic properties of SWNT, but in this thesis it will not be considered because our main focus is the mechanical properties of SWNTs.

2. SWNT Model

The initial geometric configuration of the (5, 5) armchair SWNT model needed for MD simulations are made using equations (1) and (2) together with a MATLAB

program. Figure 3 shows the side and top view of the initial (4, 4) armchair SWNT model consisting of 185 carbon atoms, which are represented by the individual spheres through the visualization MATLAB algorithm.

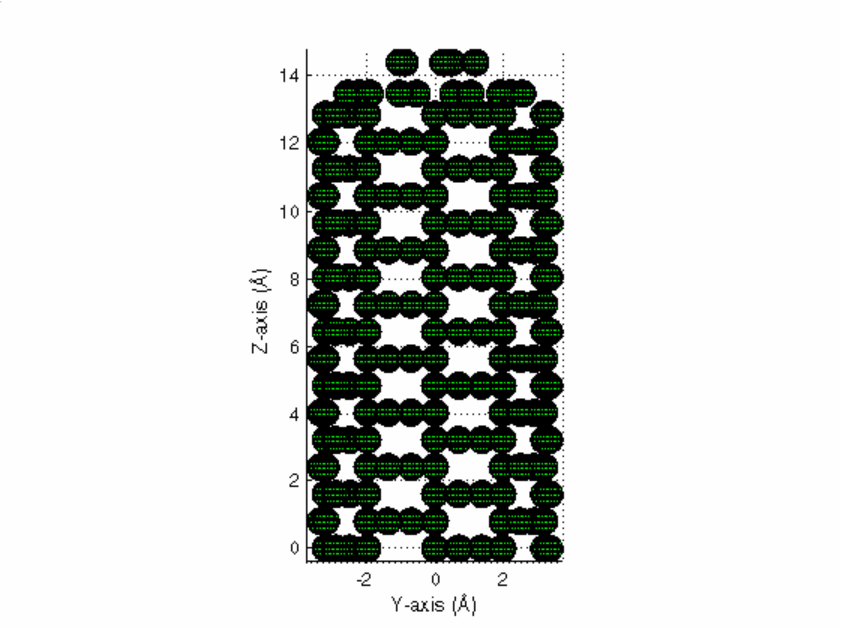

(a) Side view of the initial SWNT model

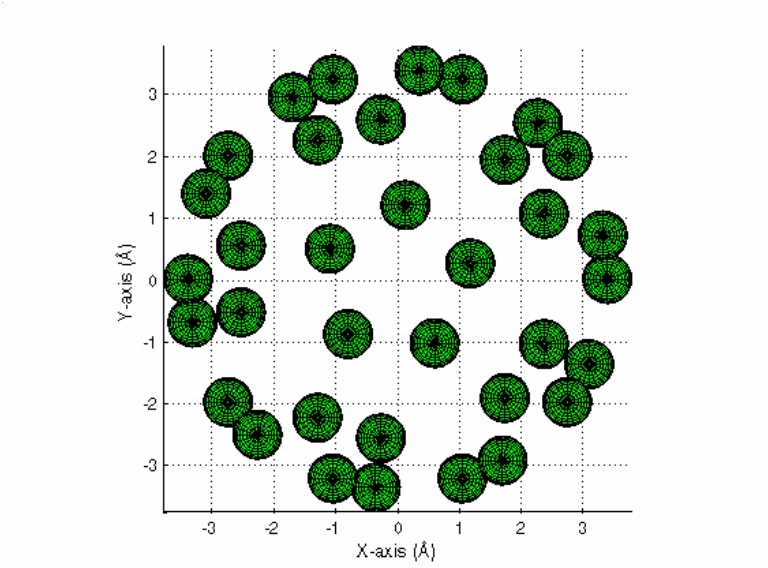

(b) Top view of the initial SWNT model

Figure 3. Initial (5, 5) armchair SWNT model from the geometrical consideration.

The average C-C distance is ~ 1.42 Å, and the diameter of the tube (x, y-axis) is 6.78 Å. The tube length (z-axis) is 14.34 Å, which was measured from the origin

coordinates (0, 0, 0) at the bottom of the SWNT to the middle tip of the end along the tube's axis. To save computational costs, the length of the SWNT model was limited to order of 10 Å. In addition, to model the half-dome shape upper cap of the SWNT, the prior investigation results were applied to this SWNT model. According to D. H. Oh *et al*., when SWNTs are formed during synthesis, a half-dome shaped cap formation is induced with pentagon defect rings, which are necessary to form the stable energy minimized structures during the cap formation mechanism of SWNT. It can be seen at the middle region of the top view in Figure 3(b) [20]. This introduced cap formation mechanism is also applied to the BSNT model.

B. SYNTHESIS POSSIBILITY AND MODELING OF BSNT

In the nanotechnology field, it is undesirable that one uses only pure nanotubes to build up embedded nano-devices or synthetic composite materials, because both mainly consist of dissimilar elements or parts. When dissimilar nanotubes are artificially connected with each other or arranged under the specific conditions, it is expected that newly formed heterogeneous nanotubes would show different physical properties. In this thesis, the Bamboo structural single-walled nanotubes (BSNT) was selected as candidate to investigate heterogeneous nanotubes based on the following two arguments

As has been mentioned, Srivastava *et al*. [14] showed two possibilities for dissimilar carbon nanotube synthesis with different diameters and chiral angles to investigate metallic and semiconductor behaviors as well as electronic transport. One possibility creating hetero-junction configurations is to connect different nanotubes through topological defects mediated junctions. In this case, the nanotubes are chemically connected with bonding networks to form a stable junction. The second possibility is that the junction is connected with a simple physical touch. A few scientists predicted that the main applications of the second method would be in electromechanical bi-stable switches and sensors [21]. The representative hetero-junction possibilities such as "Y-junctions" are shown in Figure 1(a). In that case, pairs of heptagon and pentagon ring defects are induced in a perfect hexagonal lattice structure of the original SWNTs. In particular,

those 5-7 ring pair in a hexagonal network is called “Stone-Wales (SW) defect”, which is one of the most important defective structures in CNTs that will affect Young’s modulus of the heterogeneous nanotubes.

Meanwhile, Zettle *et al*. found that outer nanotube walls or shells of multi-walled carbon nanotubes (MWNT) can be successively removed by the electronically driven vaporization of successive tube walls near the end of multi wall nanotubes (MWNT), and an inner nanotube can also be telescoped by the contacted nano-manipulator [22]. When the telescoped inner nanotube was released, it was drawn back into the outer walls by the inter-tube Van der Waals energy-lowering force. This means that nanotubes can be used for frictionless nano-springs or bearings as a part of nano-devices. Their experiment has important implications for the possibilities of controlling and shaping nanotube geometry.

The above experimental observations and theoretical predictions allow one to assume that synthesis of different SWNTs can be possible to satisfy a desirable mechanical properties of composite materials when a proper synthesis mechanism is applied under specific conditions.

For the BSNT model, let us assume that there are two SWNT as A and B with the same diameter; A can be modeled as the previous mentioned SWNT modeling method with capped ends and the closed bottom, B can also be modeled with capped ends and, instead, without the closed bottom, that is, opened bottom. When the bottom of B is physically contacted with the capped ends of A along the tube’s Z-axis with a revolved horizontal angle 0.5 radian, A and B can be jointed as a hetero-junctions through the inter-tube Van der Waals force at the junction region to lower the total system energy. When two nanotubes are coupled with horizontal joint angle of 0 radian, the hetero-junctions could not be formed during equilibrium simulation due to the chemical, geometrical bonding limits.

Based on the above arguments and assumptions, the BSNT model was generated using the MATLAB algorithm. Figure 4 demonstrates the side and top view of our BSNT

model. The two (5, 5) armchair SWNTs, upper and lower SWNT, are prepared for modeling BSNT with the average C-C distance 1.42 Å, diameter 6.78Å, and the resultant tube length of the initial BSNT model is 15.14 Å that is also measured from the origin coordinate (0, 0, 0) at bottom of the lower tube to the tip of upper tube ends along the Z-axis. The number of carbon atoms for the BSNT model is 210.

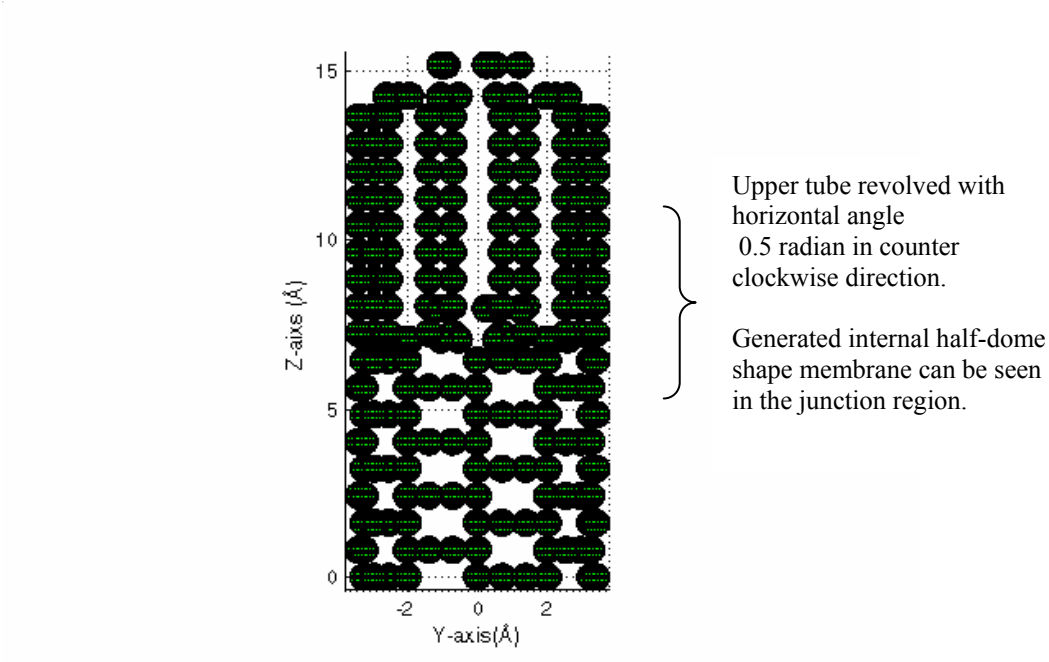

(a) Side view of BSNT model.

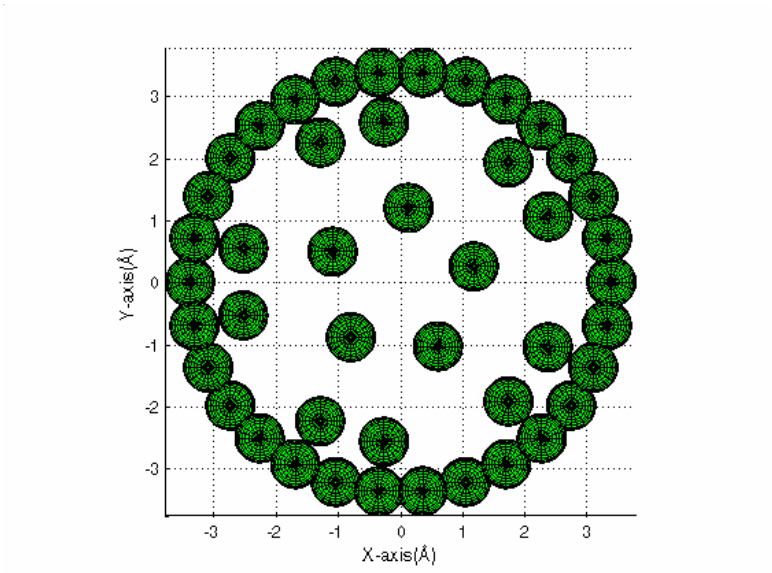

(b) Top view of BSNT model

Figure 4. The side and top view of BSNT model with 210 atoms

In Figure 4(a), since additional pentagon defect rings are introduced in the junction region, the mechanical properties of the BSNT such as Young's modulus will be different from the previous SWNT model. Therefore, if the Young's moduli of the SWNT and BSNT models can be evaluated and compared with each other from the results of the classical MD simulations, a synthesis mechanism of heterogeneous nanotubes can be investigated; thus, heterogeneous CNTs with a specific purpose could be controlled and shaped in the near future.

However, there are some restrictions on modeling the initial geometry of SWNT and BSWNT for the MD simulations through the MATLAB code. The representative constraints are computational costs such as the computational speed and modeling size. Thus, in both models, the modeled tube lengths, diameters and the total number of carbon atoms were essentially limited to save computational costs. These technical and computational problems should be solved in future research for large and realistic computer simulations. However, since the focus is to find Young's moduli of both models and to investigate mechanical deformation behaviors of small sized models, the present computational method for this thesis was assumed to be reasonable.

C. MD THEORY AND TERSOFF-BRENNER (T-B) POTENTIAL

1. Validity of the Classical MD Simulation Method

The classical molecular dynamics (MD) method is to calculate the positions and velocities of all of the molecules or atoms as functions of time within the solid, liquid, and gas state multi-particle systems, which have energetically stable structures, that is, they have minimized potential energy configurations in their systems in the equilibrium state, by using Newton's second law, Hamiltonian equation of motion, and a particular potential energy function.

As mentioned previously, sometimes the quantum mechanical MD simulation such as ab-initio method is considered being more suitable than classical MD method to simulate the exact motion of molecules or atoms within a system and to extract the

macroscopic physical properties from the microscopic observations connected with electron's influence. However, in most of cases, quantum MD simulations would be much more time consuming and computationally difficult than a classical MD simulation. Thus, the overall efficiency of MD simulation should be considered comparing which method is more suitable to investigate interesting properties. If we want to know the electronic properties of nanotubes, quantum mechanical methods would be much better than the classical MD methodd because of the influence of the embedded electron's motion. While, if we want to know only the mechanical properties of nanotubes, the classical MD method could be available to satisfy our purpose under valid conditions and assumptions.

In this thesis, the classical MD simulation method was employed to calculate the mechanical behaviors and Young's modulus of SWNT and BSWNT due to the following two distinguishable reasons. First, the De Broglie wavelength of a carbon atom at room temperature is order ~ 0.4 Å. The average spacing between carbon atoms in a solid is of order ~ 1.4 Å. Hence the atomic wavelength is smaller than the particle separation, which justifies a classical approach. Second, all of the electrons associated with each carbon atoms can be assumed to be bound tightly to their respective nuclei through the relatively strong covalent bonding network; the energy required to promote an electron to an excited state is of order 10 electron volts. This energy is much larger than the typical kinetic energy associated with the center of mass motion of an atom, which is of order 0.1 electron volts at room temperature [23]. Thus, it is a very good approximation to treat each carbon atom as a classical and simple structure-less particle. However, in large mechanical deformation simulations of CNTs, the classical approach would not be reasonable. For this reason, the tensile loading simulation for SWNT and BSNT models to study mechanical deformation behaviors will be restricted to the small strain range.

2. Newton-Hamiltonian Dynamics for the Classical MD Simulation

In the Newton-Hamiltonian Dynamics for the MD simulation, the motion of a molecule or atom i is caused by a force F_i exerted by an intermolecular potential energy

U . The motion of the atoms and applied forces are explicitly related through Newton's second law. This be called "the equation of motion of one atom", and can be written by

$$F_i = m\ddot{r}_i \qquad (3)$$

Here m is the mass of the atom; it is assumed to be independent of position, velocity, and time. The acceleration is then given by

$$\ddot{r}_i = \frac{d^2 r_i}{dt^2} \qquad (4)$$

where r_i is a vector that locates the atom with respect to the origin of the coordinate system. For a given N-atom system, Newton's second law represents 3N second-order, ordinary differential equations of motion.

For an isolated system, one conserved quantity is the total energy E . Therefore, we can identify the total energy as the Hamiltonian H . For N atoms, H takes the form

$$\mathrm{H}(r^N, p^N) = \frac{1}{2m}\sum_i p_i^2 + U(r^N) = E \qquad (5)$$

where p is the momentum of an atom and the potential energy U results from the inter-atom interactions. Taking the derivative of the above equation with respect to the distance r , the explicit relationship between the Hamiltonian and the potential energy is

$$\frac{\partial \mathrm{H}}{\partial r_i} = \frac{\partial U}{\partial r_i} \qquad (6)$$

Therefore, the resultant Hamilton's equations of motion are

$$\frac{\partial \mathrm{H}}{\partial p_i} = \frac{p_i}{m} = \dot{r}_i \qquad (7)$$

$$\frac{\partial \mathrm{H}}{\partial r_i} = -\dot{p}_i = -m\ddot{r}_i \qquad (8)$$

Using equation (6) in equation (8) and comparing with Newton's law (3) yields

$$F_i = -\frac{\partial \mathrm{H}}{\partial r_i} = -\frac{\partial U}{\partial r_i} \qquad (9)$$

From equation (9), any conservative force can be written as the negative gradient of some potential energy function U, and the forces from all of the other atoms determine the accelerations of each atom in the given system [24].

3. MDSS (Molecular Dynamics Code for Soft Sphere)

The most important aspects of a classical MD simulation code are the applied potential energy function and the finite-difference method used. The potential energy functions applied for classical MD codes are mainly categorized into soft-sphere pair potentials and hard-sphere pair potentials according to the continuity of the potential functions; the soft-sphere pair potentials represent a continuous energy function with respect to the inter-atomic distance between atoms, while the hard-sphere pair potentials are represented by a discontinuous energy function.

Most of the MD simulation codes tend to use the Verlet type algorithm or Predictor-corrector algorithm as a finite-difference method to solve the differential equations of motion numerically, because the numerical errors associated with the traditional Euler or Euler-Cromer type algorithms are too big to tolerate during the MD simulations.

The MDSS code for this research was originally developed by J. M. Haile [25] to simulate Argon atoms by introducing the Lennard-Jones potential as the soft-sphere pair potential and Gear's predictor-corrector algorithm as a finite difference method, but the original code with FORTRAN was not appropriate on simulating the carbon based

systems such as SWNT and BSNT models due to the unsuitable Lennard-Jones potential function for carbon atoms. Thus, a modified MDSS code obtained by introducing a new empirical potential function, Tersoff-Brenner type potential, was used for this thesis, and the computer program code was converted from FORTRAN code to MATLAB code due to the solidified graphical advantage of MATLAB.

4. Tersoff-Brenner (T-B) Type Potential

Dynamics for condensed matter systems such as metals and semiconductors can be described with explicit or implicit many-body force field functions using the Embedded Atom Method (EAM) type potentials for metals, and Stillinger-Weber (S-W) or Tersoff-Brenner (T-B) type potentials for semiconductors. Among them, the T-B type potentials are well parameterized from the empirical data and particularly suited for carbon based systems. It has been used in a wide variety of scenarios yielding results in agreement with experimental observations [15].

A key feature of the Tersoff-Brenner type potential is that short-range bonding interactions tend to participate readily in reactions so that chemical bonds can form and break during the MD simulations. Tersoff developed, for the first time, an analytic potential energy function based on Abell's functional forms that realistically describe bonding in silicon for a large number of solid-state structures [26, 27]. After that, from Tersoff's covalent-bonding formalism with additional terms that correct for an inherent over binding of radicals and that include non-local effects, Brenner presented a practical empirical many-body potential energy function for the hydrocarbon molecules as well as graphite and diamond lattices [28].

However, even though the original Brenner potential has been quite effective for reacting hydrocarbon molecules, it is not efficient for purely carbon atom systems because its potential function formula has a term associated with hydrogen atoms. For that reason, when the Brenner potential was coupled with the Tersoff potential, the terms associated with hydrogen atoms in the original Brenner potential were removed. Thus,

the resultant modified Tersoff-Brenner (T-B) type potential function is employed in this thesis. The T-B type potential energy as a function of the atomic coordinates is given by

$$U = \frac{1}{2}\sum_i u_i \qquad (10)$$

$$u_i = \sum_{j \neq i}[V_R(r_{ij}) - B_{ij}V_A(r_{ij})] \qquad (11)$$

where the repulsive and attractive pair terms, V_R and V_A are given by,

$$V_R(r_{ij}) = f_{ij}(r_{ij})D_{ij}^{(e)}/(S_{ij}-1)\cdot\exp(-\sqrt{2S_{ij}}\beta_{ij}(r-R_{ij}^{(e)}) \qquad (12)$$

$$V_A(r_{ij}) = f_{ij}(r_{ij})D_{ij}^{(e)}S_{ij}/(S_{ij}-1)\cdot\exp(-\sqrt{2/S_{ij}}\beta_{ij}(r-R_{ij}^{(e)}) \qquad (13)$$

where D, S, β, R are empirical parameters, and the function $f_{ij}(r)$, which restricts the pair potential to nearest neighbor atoms, is given by

$$f_{ij}(r) = \begin{cases} 1, & r < R_{ij}^{(1)} \\ \left[1+\cos\left(\dfrac{\pi(r-R_{ij}^{(1)})}{R_{ij}^{(2)}-R_{ij}^{(1)}}\right)\right]/2, & R_{ij}^{(1)} < r < R_{ij}^{(2)} \\ 0, & r > R_{ij}^{(2)} \end{cases} \qquad (14)$$

$$B_{ij} = \left[1+\sum_{k(\neq i,j)} G_i(\theta_{ijk})f_{ik}(r_{ik})\cdot\exp\left[\alpha_{ijk}\cdot((r_{ij}-R_{ij}^{(e)})-(r_{ik}-R_{ik}^{(e)}))\right]\right]^{-\delta_i} \qquad (15)$$

$$G(\theta_{ijk}) = a_0\left\{1+\frac{c_0^2}{d_0^2}-\frac{c_0^2}{\{d_0^2+(1+\cos\theta)^2\}}\right\} \qquad (16)$$

where θ is the angle between atoms $i-j$ and $i-k$ bonds and other constant variables except for distance r between carbon atoms are all parameters. These equations require a total of 11 fitting parameters for carbon atoms. The values assigned to each of these

parameters are given in Table 1, in where the subscripts "cc" means that those parameters are used for just carbon-carbon bonding network without other elements such as hydrogen.

Table 1. Optimized parameters for the T-B type potential. [28]

Parameter	Value	Parameter	Value	Parameter	Value
$R_{cc}^{(e)}$	1.42 Å	α_{ccc}	0.0	d_0^2	3.5^2
$D_{cc}^{(e)}$	6.0 eV	$R_{cc}^{(1)}$	1.7 Å		
β_{cc}	2.1 Å	$R_{cc}^{(2)}$	2.0 Å		
S_{cc}	1.22	a_0	0.00020813		
δ_{cc}	0.5	c_0^2	330^2		

The T-B potential energy function for two carbon atoms is plotted as a continuous function in Figure 5 by using the above equations (10) through (16). In an equilibrium state, two carbon atoms are separated by the equilibrium separation distance $r_0 \sim 1.42$ Å, which is called the effective carbon bond length. The equilibrium of two carbon atoms corresponds to the potential energy of the system acquiring its minimum value.

Consequently, any kind of an equilibrated CNT structure will be formed only if the potential energy per each carbon atom can attain a minimum energy value as they approach each other. This minimum energy is defined as the bond energy. The bond energy for the carbon nanotube is known to be $\varepsilon \approx 2.5eV$, which is consistent with the Carbon-Carbon tight bonding overlap energy accepted from numerous prior experiments [29, 30]. The simulated T-B potential energy as a function of interatomic separation distance from the MDSS simulation can be seen in Figure 5.

Although the above arguments are considered for only two carbon atoms, similar arguments apply to the entire bonding networks among the many carbon atoms comprising CNTs. Since any given mechanical system tends toward the minimum potential energy, the carbon atoms exert a force on each other so that they can adjust themselves to the bottom of the potential well as shown in the Figure 5. The needed force to do that is just $F = -\partial U / \partial r$ from the previous equation (9), and it is directed along the line connecting the carbon atoms.

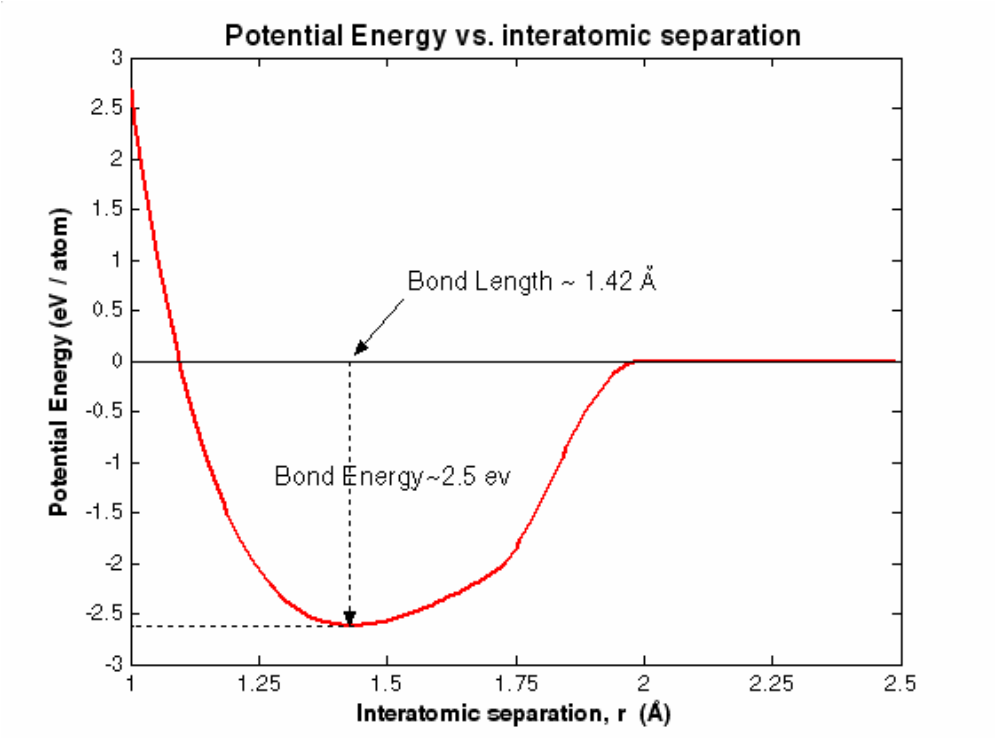

Figure 5. Potential energy vs. interatomic separation of T-B potential from MDSS code

Figure 5 shows that the T-B potential curve is asymmetric. The T-B potential curve is broader in the $r > r_0$ region. Thus, when two paired atoms are vibrating about their equilibrium positions at a given temperature, stretching and compressing the bond according to the kinetic molecular theory, the atoms will spend more time in the $r > r_0$ region, that is, more time stretching the bond than compressing the bond with respect to the equilibrium bond length r_0. However, when the temperature is approximately that of

room temperature ~300 K, the mean vibration kinetic energy is 0.039 eV (from $\frac{3}{2}kT$), and the atoms will be vibrating near the bottom of the potential well. In this case, the T-B curve can be taken as approximately symmetric, and consequently the thermal vibration motion of two atoms can be approximated as a simple harmonic oscillator motion [31, 32].

It is interesting to discuss the attractive force region because it gives us a hint for studying the deformation behaviors and Young's modulus of CNTs under an external tensile load. For the range of $1.42 < r < 2.0$ Å, the paired carbon atoms experience a significant force change when its separation reaches at around 1.72 Å; namely, the interaction force derived from the potential energy function suddenly changes from the gentle positive slope to the steep negative slope at around 1.72 Å when it goes far away from the equilibrium position as shown in Figure 6.

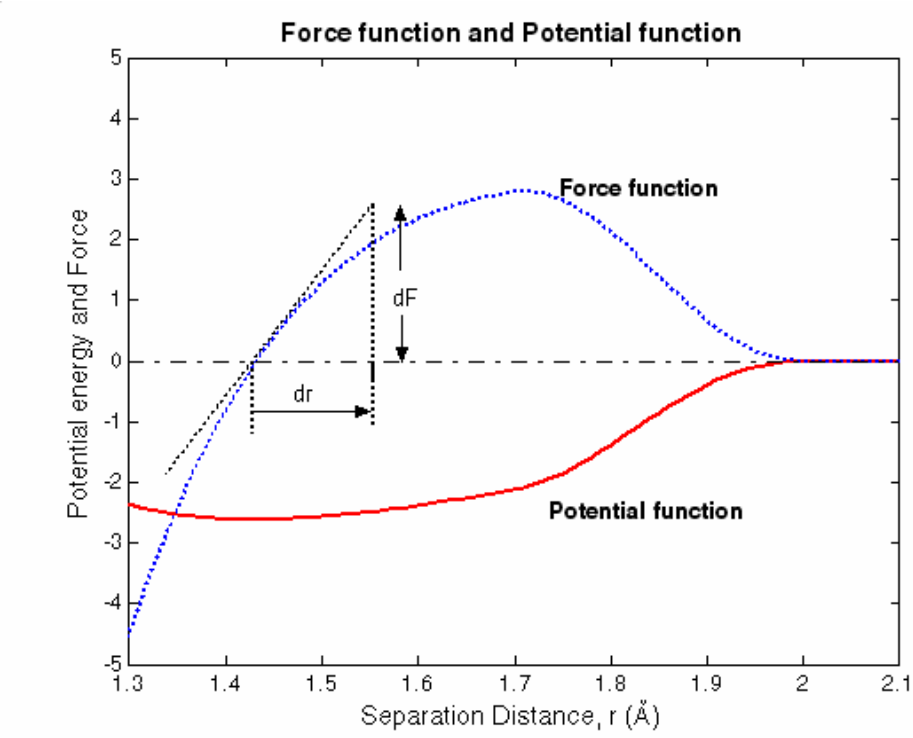

Figure 6. Idealized interaction force and potential function of one pair of carbon atoms.

Figure 6 shows the magnified parts of the attractive force region from Figure 5, and the force function is evaluated as the negative gradient of the potential energy, that is $F = -\frac{\partial U}{\partial r}$. In the above diagram, the positive Y-axis represents the attractive force region, while negative Y-axis represents the repulsive force region. At the equilibrium position r_0 the interaction force between two carbon atoms becomes zero, and then the attractive force increases until the separation distance reaches around 1.72 Å. However, as it goes away from that point, the attractive force decreases until the separation distance reaches 2.0 Å. For separations larger than about 2.0 Å, the interaction force between two atoms becomes essentially zero and this is a reason that the T-B potential is called a short range interaction potential, while for $r \le 1.42$ Å the interacting force will becomes a very strong repulsive force. Thus, from this consideration, it can be anticipated that CNTs will show a strong resistance against external compressive loads.

If a CNT is subjected to an external tensile load, the system is in a non-equilibrium state. The displacement of neighboring atoms due to the tensile force results in a net attractive force, and subsequently this net force will be balanced by a portion of the applied force acting on these atoms. According to Kasap, Young's modulus can be evaluated by the measurement of the above balance [33]. Thus, the Y value depends on the gradient of the interaction force F versus separation distance r at the equilibrium position r_0 as shown in Figure 6, and can be written

$$Y = \frac{1}{r_0} \cdot \left[\frac{\partial F}{\partial r} \right]_{r=r_0} \qquad (17)$$

Based on equation (17), the computer generated Y value was 16.74 TPa when r_0=1.42 Å. This unrealistically high Young's modulus is due to the consideration of the idealized one pair of carbon atoms. That is, there is no special effect of many-body interaction forces. Therefore, a realistic Young's modulus of CNT system can be found

only when we consider the many-particle interaction forces including the bonding angle effect that is represented as the G function within the previously mentioned T-B potential function.

Meanwhile, it is geometrically impossible for every pair of carbon atoms in a carbon nanotube system to be at separations corresponding to the minimum energy. Moreover, the thermal energy, which is manifested as interactions among atoms, constantly knock atoms pairs away from the minimum-energy separation, and the overall behavior of the collection of atoms, therefore, may be quite complex. Thus, it is expected that the actual Young's modulus of CNTs will converge to a realistically accepted value, the order of ~ 1 TPa, when all the facts mentioned above are coupled at the same time and the modified MDSS simulation is applied to the CNTs model system.

5. Gear's Predictor-Corrector Method for Solving the EOM

For solving the differential equation of motion of the many-particle system numerically, several methods are possible. The Verlet method or Euler-Cromer method is one of the simplest finite differences approaches. However, in molecular dynamics, the motion of a particle is computed over a very large number of time steps, and it turns out that the numerical errors associated with above two type methods are too big to tolerate. It is, therefore, necessary to use a slightly more complicated scheme for solving the differential equations arising from Newton's second law and Hamiltonian dynamics. The scheme adopted in this thesis is known as Gear's Predictor-Corrector method [34].

Gear's method is composed of three steps: prediction, evaluation, and correction. Since it is important to understand the process of the error accumulation with the simulation time step as the MDSS code simulation runs, details of this method are presented here. The equations below will give the ith carbon atom the required information to calculate the trajectories, such as the position r_i, velocity $\dot{r}_i$, and acceleration $\ddot{r}_i$ at time $t + \Delta t$.

a. Prediction

A carbon atom's position at time $t + \Delta t$ is predicted using a fifth-order Taylor series based on the positions and their derivatives at time t.

$$r_i(t+\Delta t) = r_i(t) + \dot{r}_i(t)\Delta t + \ddot{r}_i(t)\frac{(\Delta t)^2}{2!} + \dddot{r}_i(t)\frac{(\Delta t)^3}{3!} + r_i^{(4)}(t)\frac{(\Delta t)^4}{4!} + r_i^{(5)}(t)\frac{(\Delta t)^5}{5!} \qquad (18)$$

$$\dot{r}_i(t+\Delta t) = \dot{r}_i(t) + \ddot{r}_i(t)\Delta t + \dddot{r}_i(t)\frac{(\Delta t)^2}{2!} + r_i^{(4)}(t)\frac{(\Delta t)^3}{3!} + r_i^{(5)}(t)\frac{(\Delta t)^4}{4!} \qquad (19)$$

$$\ddot{r}_i(t+\Delta t) = \ddot{r}_i(t) + \dddot{r}_i(t)\Delta t + r_i^{(4)}(t)\frac{(\Delta t)^2}{2!} + r_i^{(5)}(t)\frac{(\Delta t)^3}{3!} \qquad (20)$$

$$\dddot{r}_i(t+\Delta t) = \dddot{r}_i(t) + r_i^{(4)}(t)\Delta t + r_i^{(5)}\frac{(\Delta t)^2}{2!} \qquad (21)$$

$$r_i^{(4)}(t+\Delta t) = r_i^{(4)}(t) + r_i^{(5)}(t)\Delta t \qquad (22)$$

$$r_i^{(5)}(t+\Delta t) = r_i^{(5)}(t) \qquad (23)$$

b. Evaluation

The intermolecular force F_i on each atom is calculated at time $t + \Delta t$ using the predicted positions. The evaluation of the forces is the most time consuming process. The force on each molecule is given by the potential energy function as

$$F_i = -\sum_{j \neq i} \frac{\partial U(r_{ij})}{\partial r_{ij}} \qquad (24)$$

where $U(r_{ij})$ is continuous potential energy function that acts between atoms i and j.

c. Correction

The predicted positions and their derivatives are corrected by using the discrepancy $\Delta\ddot{r}_i$ between the predicted acceleration and that given by the evaluated force F_i.

$$\Delta\ddot{r}_i = \left[\ddot{r}_i(t+\Delta t) - \ddot{r}_i^{P}(t+\Delta t)\right] \qquad (25)$$

In Gear's algorithms for second-order differential equation of motion, this difference term is used to correct all predicted positions and their derivatives; this method is introduced in reference [34].

6. Simulation Time Step

In our modified MDSS code, the simulation is propagated through time at intervals of Δt by iterating the above 3 steps (prediction-evaluation-correction) in Gear's method at every time step. Since based on the energy conservation principles, typically Gear's algorithm is known that it is about one order higher in accuracy than Verlet's. A reasonable simulation time step Δt for our modified MDSS code was estimated as 0.01 ps using the relation between the bond length r_0 and the bond energy ε as shown in Figure 5. The method to find the reasonable time step size is presented below.

For the isolated system, the kinetic energy of an atom should be about the same as the potential energy of the atom. Let us assume that one atom can move within the bond length r_0 during the time step Δt. Then, the kinetic energy E_k and the velocity v of the atom is written by

$$E_K = \frac{1}{2}mv^2 = \varepsilon \qquad (26)$$

$$v = \frac{r_0}{\Delta t} \qquad (27)$$

From equations (26) and (27), we can calculate the maximum possible Δt value as

$$\Delta t = r_0\sqrt{m/2\varepsilon} \le 0.02 \text{ ps} \qquad (28)$$

where m is the mass of the carbon atom, and r_0 and ε are the carbon bond length and C-C tight bonding overlap energy. Based on equation (28), the time step 0.01 ps used for the MDSS code could be considered as a reasonable value.

D. FREESTANDING THERMAL VIBRATION METHOD

This section describes the method to calculate Young's modulus of SWNT and BSWNT by introducing the freestanding room temperature vibration method presented by Krishnan et al [16]. According to the kinetic molecular theory, carbon atoms are vibrating about their equilibrium positions with a mean vibration kinetic energy that increases with the temperature as $\frac{3}{2}kT$. From this fundamental principle, Krishnan et al estimated the Young's modulus of single-walled carbon nanotubes as $< Y >= 1.25 - 0.35/+0.45$ TPa by observing SWNT's freestanding room temperature vibrations in a transmission electron microscope (TEM).

Their formula to calculate Young's modulus was derived from the relationship between the motion of a vibrating clamped cylindrical cantilever rod governed by the classical fourth-order wave equation and the quantum mechanics-statistical probability theory given by the Boltzmann factor. The resultant relationship between Young's modulus Y, length L, inner and outer tube radii b and a that forms a cylindrical carbon nanotube wall, and the *rms* displacement σ, which is represented by the vibration amplitude at the tip of a carbon nanotube at a temperature T, can be expressed by

$$\sigma^2 = 0.8486\frac{L^3kT}{YWG(W^2+G^2)} \qquad (29)$$

where W is the single-walled carbon nanotube width (diameter), $G(=a-b)$ is the graphite interlayer spacing of 0.34 nm, and k is the Boltzmann constant.

For the purpose of this thesis, we have used equation (29) to predict the Young's modulus,

$$Y = 0.8486\frac{L^3 kT}{\sigma^2 WG(W^2+G^2)} \qquad (30)$$

From this equation, it should be noticed that Young's modulus depends strongly on the rms displacement σ at the tip of the SWNT for a given length and width W of the carbon nanotube and the given ambient temperature T.

How far will a carbon atom at the tip of SWNT or BSWNT vibrate in a given parameter such as time interval, diameter, and temperature? In the 3-D Cartesian, coordinates {X, Y, Z}, a position vector r_i that locates carbon atom i in a system (or our model) is defined by three linearly independent vectors as

$$\vec{r}_i = X\vec{x} + Y\vec{y} + Z\vec{z} \qquad (31)$$

If the atoms are allowed to move from their equilibrium positions by an amount of displacement vector $\vec{u}_i = (u_{ix}, u_{iy}, u_{iz})$ at a time t_0, then the actual position at the time of any carbon atom under the influence of a vibration (thermal fluctuation) is given by

$$\vec{R}_i(t_o) = \vec{r}_i(t_o) + \vec{u}_i(t_0) \qquad (32)$$

After a time interval t, the changed position of atom can be written as

$$\vec{R}_i(t) = \vec{r}_i(t_o) + \vec{u}_i(t) \qquad (33)$$

From equation (32) and (33), we can find the mean square displacement msd of carbon atom i at the tip of SWNT at given time t. It is defined by

$$msd_i(t) = \left\langle (\vec{R}_i(t) - \vec{R}_i(t_0))^2 \right\rangle \qquad (34)$$

where the notation <… > denotes here averaging over all the aotms.

When this quantity is averaged over all N atoms consisting of the end tip of the SWNT or BSNT, the rms displacement σ of the carbon nanotube-tip can be written as

$$\sigma = \left(\frac{\sum_{i=1}^{N} msd_i(t)}{N} \right)^{1/2} \qquad (35)$$

In MDSS simulation to find Young's modulus for SWNT and BSNT models under the equilibrium state, the above equations (31) ~ (35) play an important role to calculate the numerical rms displacement values from the simulated trajectory data of the carbon atoms, which were then applied in equation (30) to compute the Young's modulus.

THIS PAGE INTENTIONALLY LEFT BLANK

III. RESULTS AND DISCUSSION

A. EQUILIBRIUM AND VIBRATION MOTION OF SWNT AND BSNT

The system with atoms randomly assigned initial velocities taken from a Gaussian distribution must be allowed to reach equilibrium before any reliable measurements could be taken. In this thesis, equilibrium was monitored using the Boltzman H-function that represents the instantaneous velocity distribution; the distribution at one moment during the simulation. The corresponding value of the H-function for the x-component can be written as,

$$H_x(t) = \int_{-\infty}^{\infty} f(v_x) \ln f(v_x) dv_x \qquad (36)$$

where $f(v_x)dv_x$ is the Maxwell's velocity distribution, which is the fraction of atoms having velocities between v_x and $v_x + dv_x$, and can be evaluated analytically, giving

$$f(v_x)dv_x = \sqrt{\frac{m}{2\pi kT}} \exp\left(\frac{-mv_x^2}{2kT}\right) dv_x \qquad (37)$$

Based on the Boltzman's H-theorem, H-function decreases from an initial value to its value given by the Maxwell velocity distribution equation (37) until the system reaches equilibrium. Once equilibrium is attained, the H-function will show steady-stable fluctuations with respect to an average value [35]. Figure 7 (a) and (b) shows the simulated H-function for our SWNT and BSNT model from the initial to the equilibrium states, respectively. Both H-functions converged to some values, and they became steady at something close to that. It is an indication that equilibrium of both systems has been achieved. In Figure 7, the H-function of BSNT model displays more fluctuations than that of SWNT model within the same range of time step as 200 ~ 400, in which the minimized potential energy of both models are observed. This indicates that, though both models reached the equilibrium state after the order of ~200 time steps running, the fluctuation of carbon atom velocities in BSNT model is larger than in the SWNT model.

As a result, it may be expected that Young's modulus of BSNT should be lower than SWNT under the same temperatures and constraints, because the atomic *rms* displacement σ of BSNT model is expected to be larger than SWNT by the relation between Y and σ in equation (30).

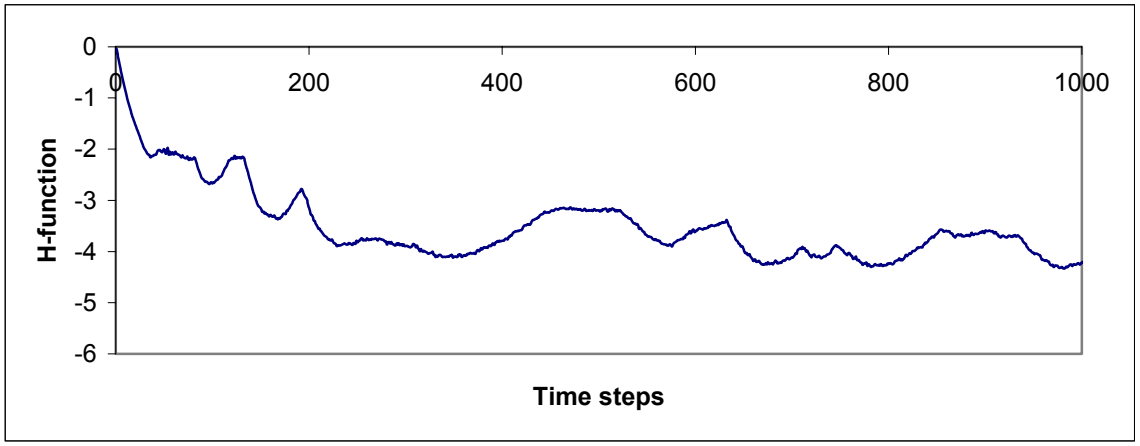

(a) SWNT model's H-function with time steps

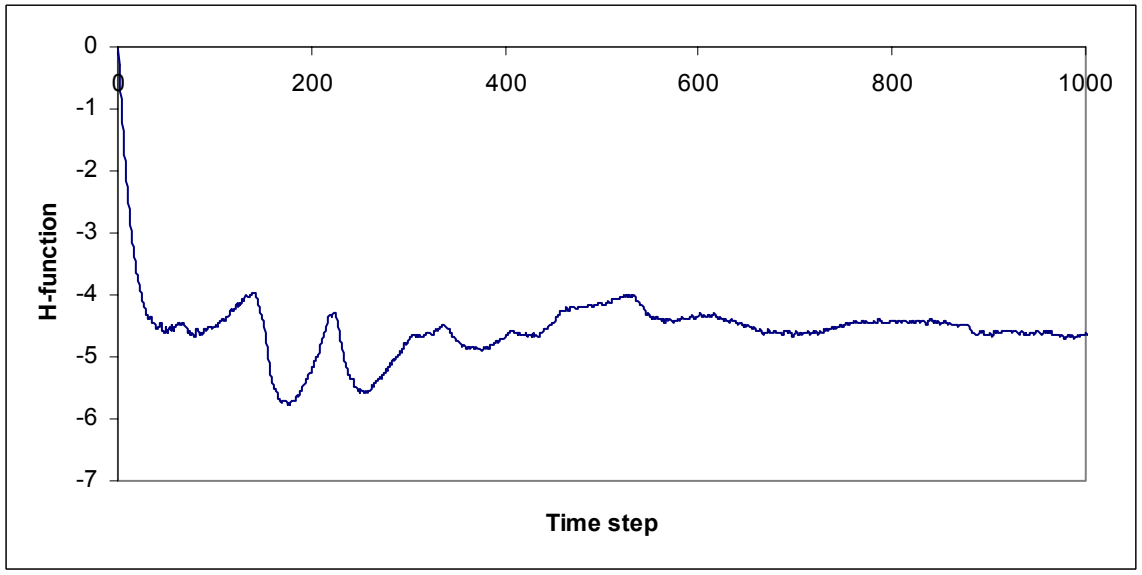

(b) BSNT model's H-function with time steps

Figure 7. H-function of SWNT and BSNT model from MDSS simulation.

Figure 8 (a) and (b) shows the equilibrated side and top configuration of the armchair (4, 4) SWNT model made of 185 carbon atoms after the equilibrium MDSS

simulation. The configuration was captured when the potential energy per carbon atom of SWNT model reached the minimum value and atoms were vibrating about the equilibrium state. In the center of Figure 8(b), the local topology of the cap region of the SWNT model, which has a pentagon defects ring pole, can be seen. According to Y. H. Lee et al, this pentagon topology becomes a seed for the stable cap formation mechanism of SWNT model [20]. They are our key objects to calculate Young's modulus of SWNT model using the thermal vibration method, because they consist of the tip of SWNT model. A few atomic vibration motions along the circumference of SWNT model, which was not observed in the initial configuration in Figure 3(b), can be seen in Figure 8(b). In particular, when the top view of Figure 8 (b) is compared with its initial configuration as shown in Figure 3 (b), an evenly distributed atoms configuration at SWNT tip is observed because each carbon atom in that region is looking for the atomic position having the minimum potential energy, already mentioned in previous sections with the potential function diagram in Figure 5 and 6.

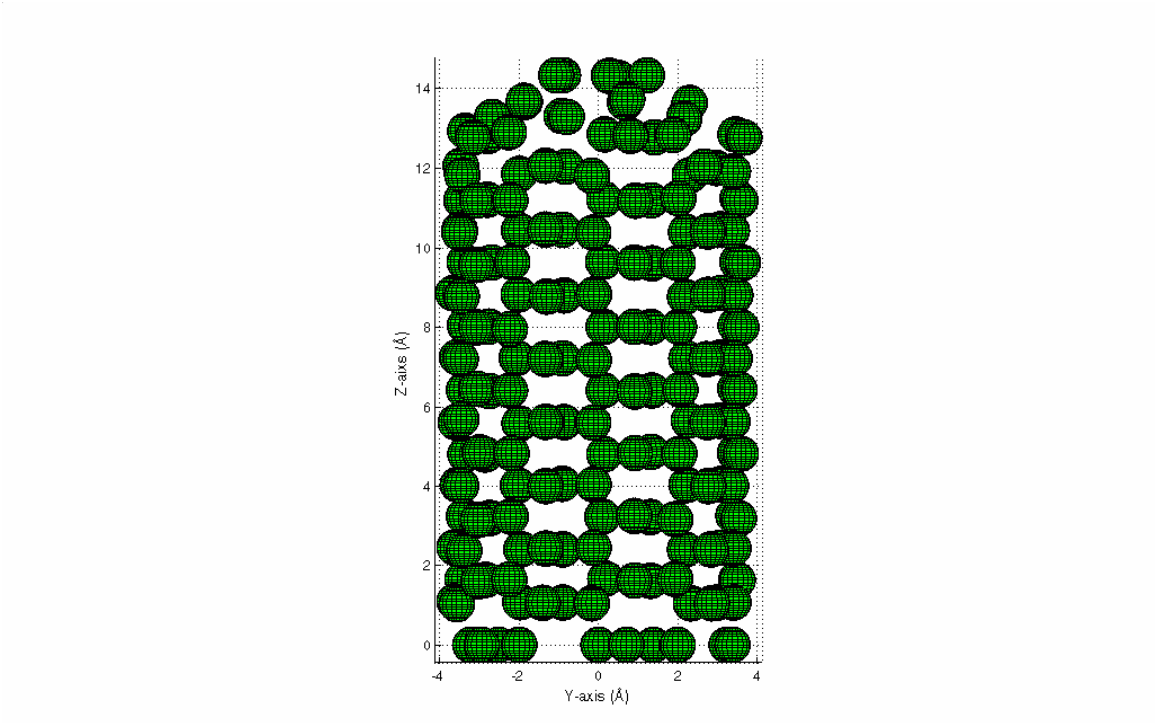

(a) Side view of SWNT model under the equilibrium

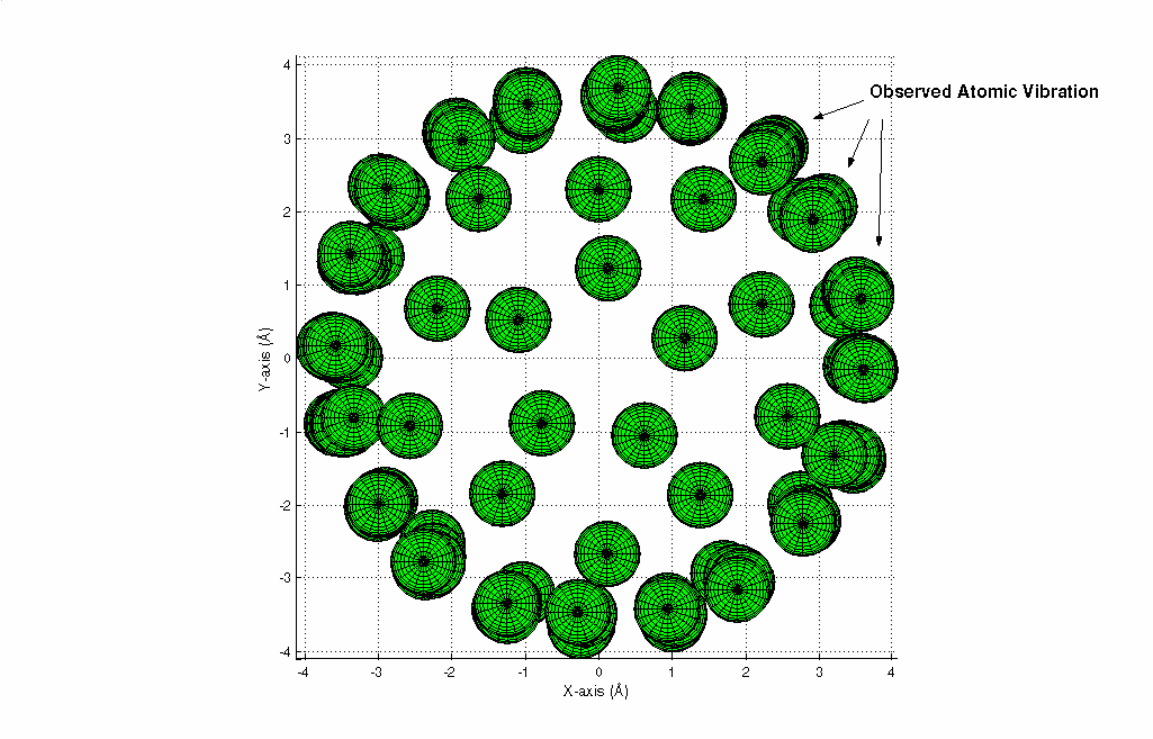

(b) Top view of SWNT model under the equilibrium

Figure 8. The side and top view of SWNT model under the equilibrium.

On the other hand, the equilibrated configurations for the BSNT, which consists of two armchair (5, 5) SWNTs and total 210 carbon atoms, are shown in Figure 9. The equilibrium process for the BSNT model is similar to the previous SWNT model. Figure 9 (a) and (b) show the equilibrated side and top views. The equilibrated BSNT model showed somewhat different features with respect to the SWNT model. The remarkable local-topology changes such as knot-shaped defects that look like protuberant lumps at a point from which a stem or branch grows, were created at the hetero-junction region along the circumference of BSNT. The atomic vibrational motions are also observed, but the magnitudes of those are more conspicuous than SWNT model. In both cases, the central pentagon ring of the end-tip of both models did not show visible vibration motions because it was difficult to catch the *rms* displacements of those pentagon ring's atoms by eye on the atomic scale. Thus, to find the atomic scale's displacements of end-tips of both models, computer algorithms were developed for calculating Young's modulus by using the equations (32) ~ (35).

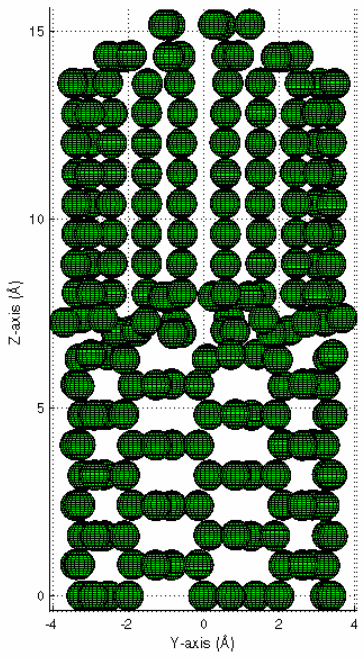

(a) Side view of BSNT model under the equilibrium

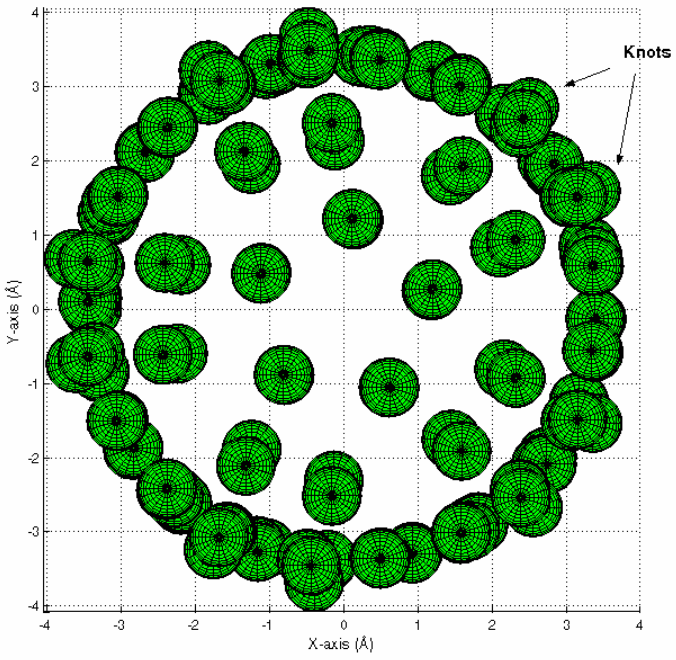

(b) Top view of BSNT model under the equilibrium

Figure 9. The side and top view of BSNT model under the equilibrium.

B. YOUNG'S MODULI OF SWNT AND BSNT MODEL UNDER EQUILIBRIUM

The two models generated in the preceding section were tested under the equilibrium MDSS simulation at room temperature 300 K, and then Young's moduli of SWNT and BSNT were evaluated based on equations (30) and (35). After that, the numerical values were compared with the theoretical and experimental results presented from other studies.

Figures 10 (a) and (b) show the histograms to demonstrate the spread in the evaluated Young's modulus values for the SWNT and BSNT by running each 100 simulations, and measured objects were the carbon atoms of the pentagon ring pole at the tip in both models. The MDSS code was designed to calculate the *rms* displacements of the tip carbon atoms using equations (31) ~ (35) when the instantaneous kinetic energy per atom of both models reached 0.039 eV ($\sim\frac{3}{2}kT$) at given room temperature $300K$. Then, Young's modulus was calculated using equation (30). In both cases, the use of 100 simulations was considered sufficient to reduce statistical errors due to the random initial velocities for both models.

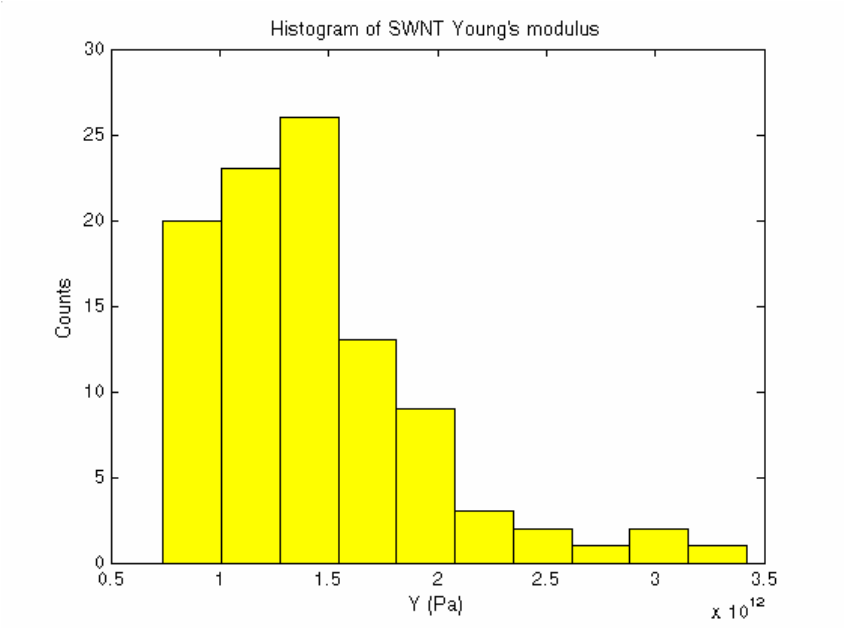

(a) Histogram of SWNT Young's modulus

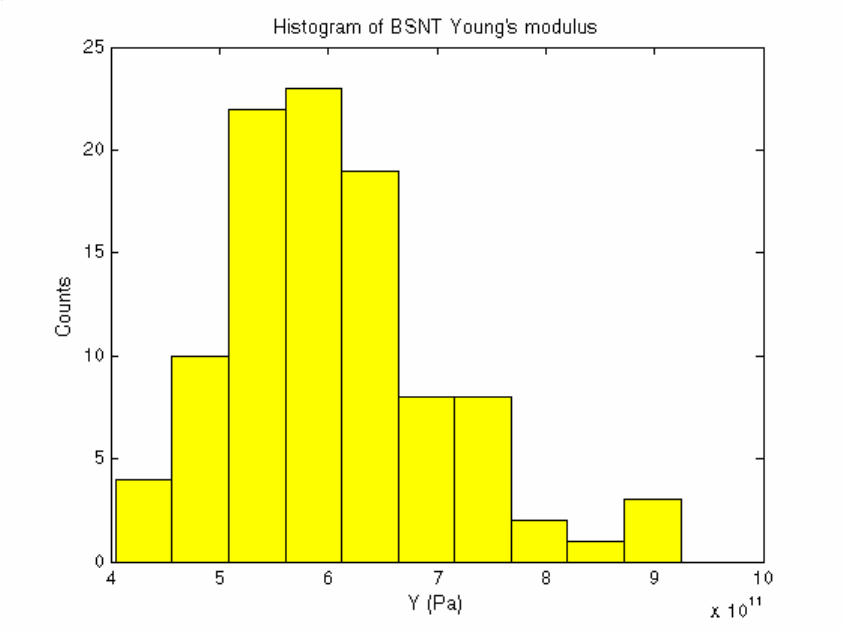

(b) Histogram of BSNT Young's modulus

Figure 10. Histogram of SWNT and BSNT Young's modulus from MDSS.

The observed distributions of Figure 10 (a) and (b) are fairly asymmetrical about the mean values, displaying a tail extending to higher values. These asymmetrical distributions could affect the ability to interpret the reliability of a mean Y value without a normal distribution assumption, because most of the measured data have experimental errors. Thus, under the equilibrium MDSS simulation, there are essential embedded random errors during the simulation process due to the time evolution method and different initial conditions on each independent simulation such as random initial velocities. Though embedded time evolution errors in MDSS code can not be completely removed, a normal distribution assumption about the randomly distributed Y values evaluating from MDSS results is feasible due to the fact that the assigned initial velocities are normally distributed by the Maxwell-Boltzman velocity distribution.

According to the assumption that the measured Young's modulus shows a normal distribution about a mean value, a normal probability density functions for the SWNT and BSNT model can be computed. The normal probability density function for a random

variable x [36], which represents the Young's modulus value, with mean μ and standard deviation σ is given by,

$$f(x) = \left(\frac{1}{\sigma\sqrt{2\pi}}\right) \cdot \exp\left\{\frac{-(x-\mu)^2}{(2\sigma^2)}\right\}, \quad \text{where } -\infty \le x \le +\infty \qquad (38)$$

The parameters used for this normal probability density function for the computed Young's moduli are shown in Table 2. The data were colleted from the equilibrium MDSS simulation results of SWNT and BSNT model.

Table 2. Statistical data measured from MDSS simulations of SWNT / BSNT model.

Parameter	SWNT	BSNT
Number of Simulations	100	100
Mean Young's modulus (TPa)	1.4243	0.6041
Standard deviation (TPa)	0.342	0.1002
Max Y value (TPa)	3.4202	0.9241
Min Y value (TPa)	0.7402	0.4046

Figure 11 shows the normal probability density functions of both SWNT and BSNT model plotted by using equation (38) with the parameters of Table 2. The mean value of Young's modulus for SWNT model was 1.42 TPa with the standard deviation of 0.34 TPa. Based on this data, the expected mean Young's modulus for the real population of SWNT can be predicted as 1.42 ± 0.23 TPa with 50 % confidence intervals. These values are in good agreement with the theoretical and experimental Young's modulus values reported by others as shown in Tables 3 and 4 [14].

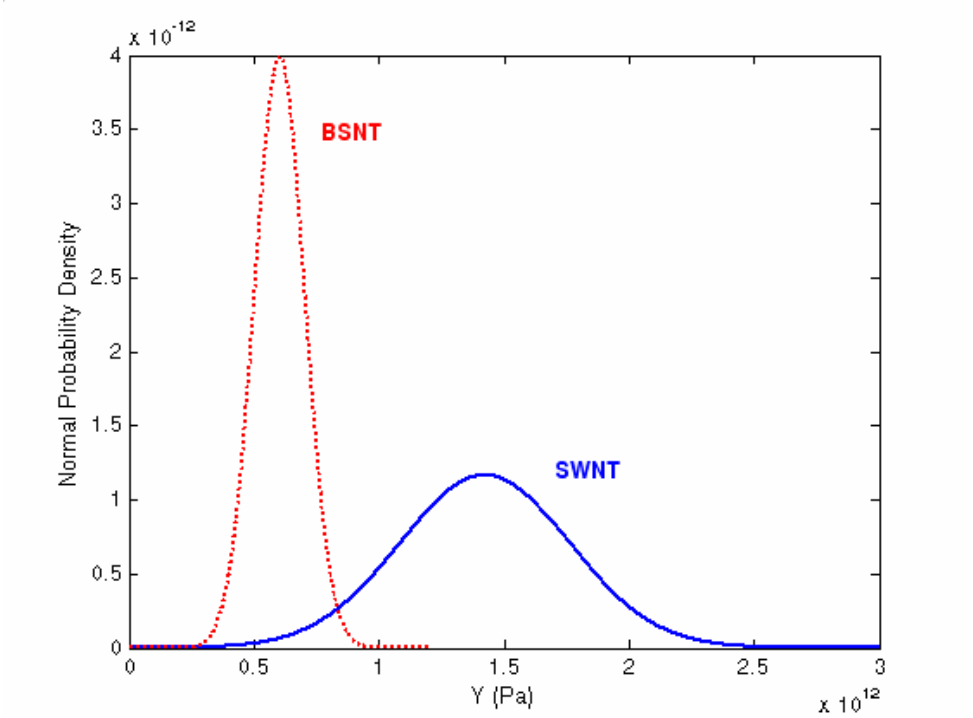

Figure 11. Normal probability density functions of Y values for SWNT and BSNT.

Table 3. Various theoretical calculations for Young's modulus
(Y: Young's modulus, h: the CNT wall thickness)

Method	Molecular dynamics Terssoff-Brenner force field [37]	Empirical force constnat model [38]	Non-orthogonal tight-binding [39]	Ab initio DFT [40]
h	0.06 nm	0.34 nm	0.34 nm	0.34 nm
Y	SWNT: 5.5 TPa	SWNT: 0.97 TPa	SWNT: 1.2 TPa	SWNT rope: 0.8 TPa, MWNT: 0.95 TPa

Table 4. Various experimental studies for Young's modulus
(Y: Young's modulus, h: the CNT wall thickness)

Method	Thermal Vibration [41]	Restoring force of bending [42]	Thermal Vibration [43]	Deflections Forces [44]
h	0.34 nm	0.34 nm	0.34 nm	0.34 nm
Y	MWNT: 1.8 ± 1.4 TPa	MWNT: 1.28 ± 0.59 TPa	SWNT: 1.3 -0.4/+0.6 TPa	SWNT: 1.0 TPa

In particular, considering about 48% of Y values for the SWNT model, which were distributed within the range 1.0 ~ 1.5 TPa as shown in Figure 10(a), and comparing with the previously mentioned mean Young's modulus of SWNT, <1.25 TPa> as evaluated by the same thermal vibration method presented by Krishnan *et al*. as shown in Figure 12, which demonstrates a histogram of Young's modulus obtained from the real 27 SWNTs, the consistency of both results are comparable. In their method, the tube's length and tip vibration amplitudes were estimated directly from the digital micrographs (TEM images). From these consistent results, the MDSS simulation was reasonable to be used for evaluating Young's modulus of SWNT model, and it may be feasible to simulate BSNT model.

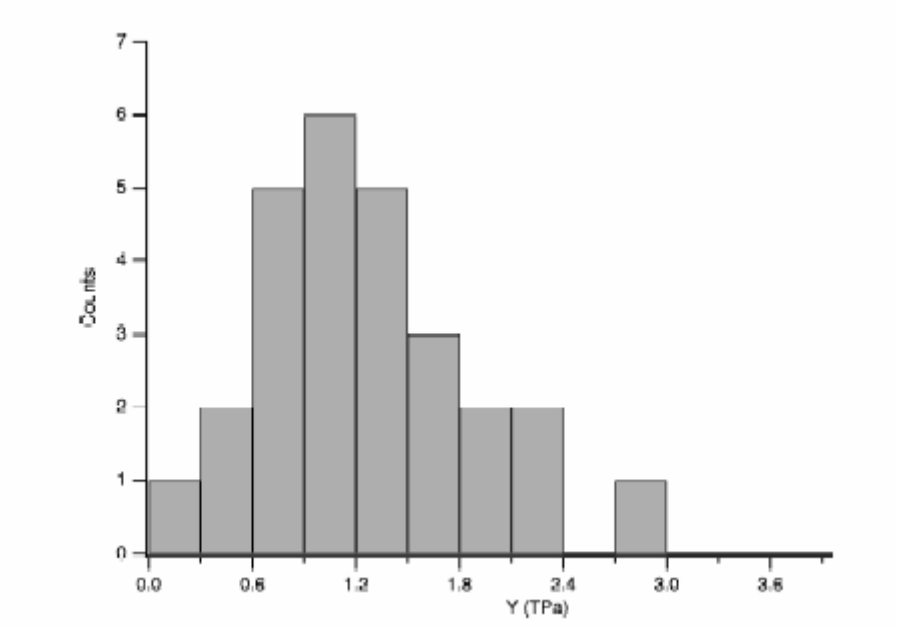

Figure 12. Histogram of SWNT Young's modulus obtained by Krishnan *et al* [43].

The equilibrium MDSS simulation results of the SWNT and BSNT models shows two important features. One is that though SWNT MDSS results and prior studies are consistent with each other within the mean error, the Y value (mean 1.42 TPa) of SWNT model calculated from MDSS simulation shows a somewhat higher value than the Y values (mean 1.25 TPa) used with the same thermal vibration method reported by Krishnan *et al.* [16]. A second is that the calculated Y value of BSNT model shows an

obvious difference with respect to the SWNT model as shown in Figure 12. The mean Y value of BSNT model was calculated as 0.604 TPa with a standard deviation 0.1 TPa. Consequently, if BSNT can be synthesized in practice, the expected mean Young's modulus for a real BSNT population would be predicted to be 0.604 ± 0.07 TPa with a 50% confidence level. Contrary to general belief that expects high Y values due to the fact that the BSNT has an internal support structure, our results show a significantly lower Y value than that of SWNT, but it still shows a strong Young's modulus comparing with other materials such as a hardened steel of the order of 210 GPa [45]. Unfortunately, so far there are no available data for the heterogeneous CNT's Young's moduli to be compared with the Y value of the BSNT model. Nevertheless, it might be expected that this thesis may play a starting role to speed up the progress of heterogeneous type nantotube synthesis in further study of the nanotechnology field.

One reason for a somewhat higher mean Y value of SWNT model calculated from MDSS simulation can be understood from the parameter relationships of the previous equation (30).

$$Y = 0.8486 \frac{L^3 kT}{\sigma^2 WG(W^2 + G^2)} \qquad (30)$$

In this equation, the Y value is inversely proportional to the width of the carbon nanotubes W when the other parameters are held the same. This means that the Y value of CNTs has the dependence on the diameter of the tube [38]. Krishnan *et al.* used the nanotube widths as a range of 1.0 ~ 1.5 nm (10 ~15 Å) to calculate Young's modulus by using equation (30), while our SWNT and BSNT model diameter used in MDSS simulation is just 6.78 Å. Therefore, it is natural to expect that measured Young's modulus of SWNT model (mean 1.45 TPa) in MDSS is higher than Krishnan's Young's modulus (mean 1.25 TP a) from the above fundamental relations.

There is another possible factor in explaining the difference in the Y values between our MDSS results and the prior experimental results reported by others. In most

of the prior experiments, the CNTs were not only made of carbon atoms, but also had impurities due to the limit of SWNT'S synthesis process in practice. Typically, it is known that impurities contained in CNTs lower their mechanical strength. Thus, it is a reasonable inference that the Young's modulus evaluated from the MD simulation using the SWNT model made of pure carbon atoms may have a higher strength than real CNTs.

On the other hand, why is the Y value of the SWNT model higher than BSNT model with roughly twice as shown in Figure 12? Earlier studies reported that the Yong's modulus of CNTs probably depends on the presence of structural imperfections such as the nesting of tubular cylinders, which can create a joint or "knuckle" thereby weakening the tube, and structural defects with the pentagon (5) – heptagon (7) rings. In the BSNT model shown Figure 9 (b), the appeared defects along the circumference of the BSNT model can prove the arguments presented by D. Srivastava *et al*. in reference [14]; when heterogeneous CNTs are formed, the 5-7 defect rings are induced, and the induced defects absorb a partial energy from the total energy of system because it requires a defect formation energy.

Thus, the defects at the junction regions of BSNT model may absorb energy, with other region's energy per atom increasing to be balanced so that the total energy of an isolated system is constant. As a result, the energy needed for the atomic vibration in the BSNT tips would increase, and then the Young's modulus of the BSNT model would be lower than that of the SWNT model based on the relationship of equation (30). This analytical interpretation is also consistent with the results of Figure 7(b) as mentioned previously. However, it is not clear which energy, namely kinetic or potential energy has an important role for that mechanism. Further analysis of the energetic in conjunction with the quantum mechanics should be considered to solve that problem.

C. TENSILE DEFORMATION BEHAVIORS OF SWNT AND BSNT MODEL UNDER NON-EQUILIBRIUM

The deformation behaviors of SWNT and BSNT under an external tension load were simulated with the MDSS code to compare the Young's modulus of both models. When a system is subjected to an external perturbation, the system is forced out of

equilibrium. When using the MDSS code to simulate trajectories of atoms through phase space, an alternative equation of motion (EOM) is needed to force the system from equilibrium. By adding additional terms of external forces to the original equilibrium EOM described in the previous sections, the equilibrium system could be coupled to the tensile loads. Series of the MDSS simulation plots of tension at the nano-scale are presented to investigate the mechanical behaviors and reactions of both models.

Figures 13 (a~d) and 14 (a~d) are MDSS simulation plots of the axial tensile loading test performed on both models at various forces of 3 ~ 60 (nN/atom), respectively. Figures 13(a) and 14(a) show the initial set-up of the SWNT and BSNT after the equilibrium relaxation. The bottom atoms of both models are constrained as if they are anchored at a substrate material. Then, various Z-direction tensile forces were applied to the carbon atoms in the cap region of both SWNT and BSNT such as a conventional tensile specimen.

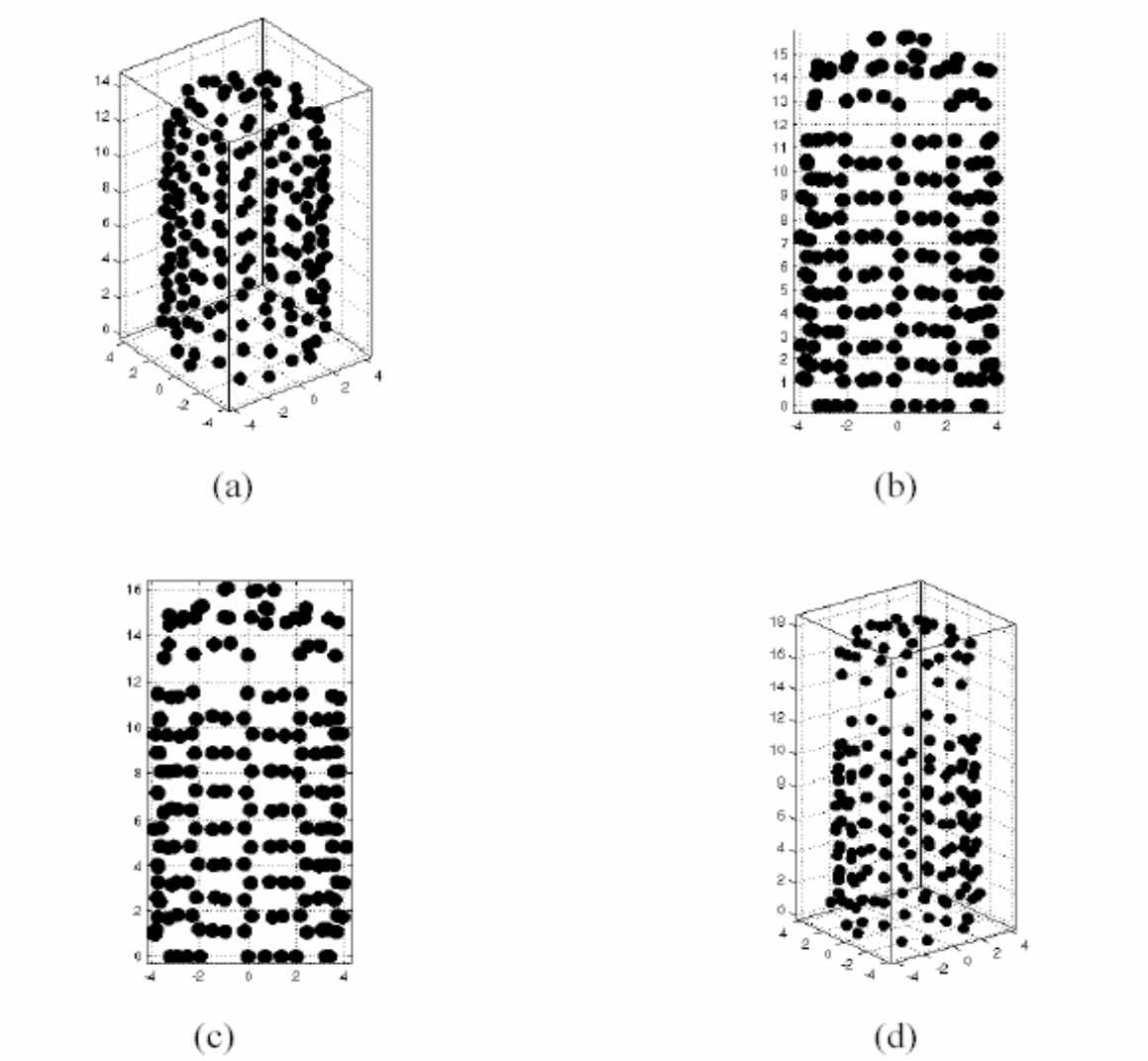

Figure 13. Configurations of SWNT model using non-equilibrium MDSS simulation.

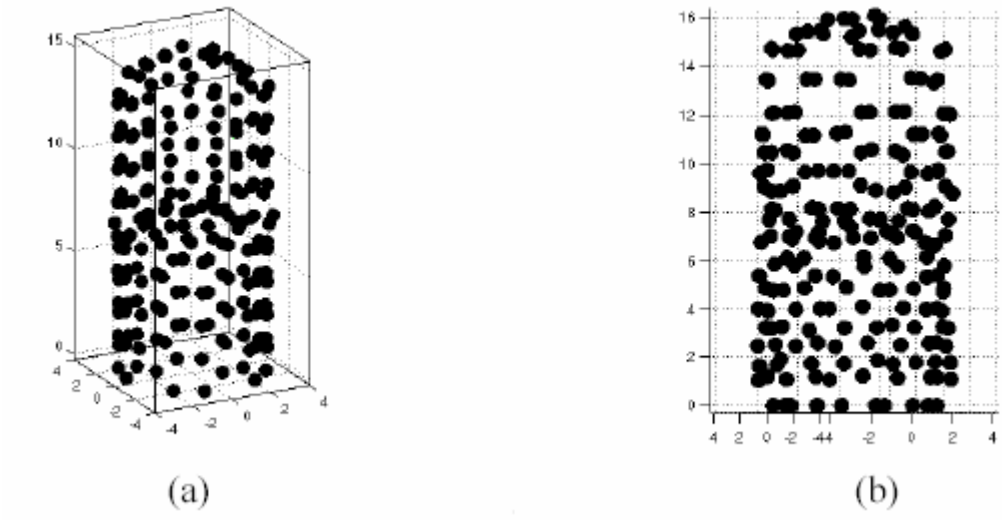

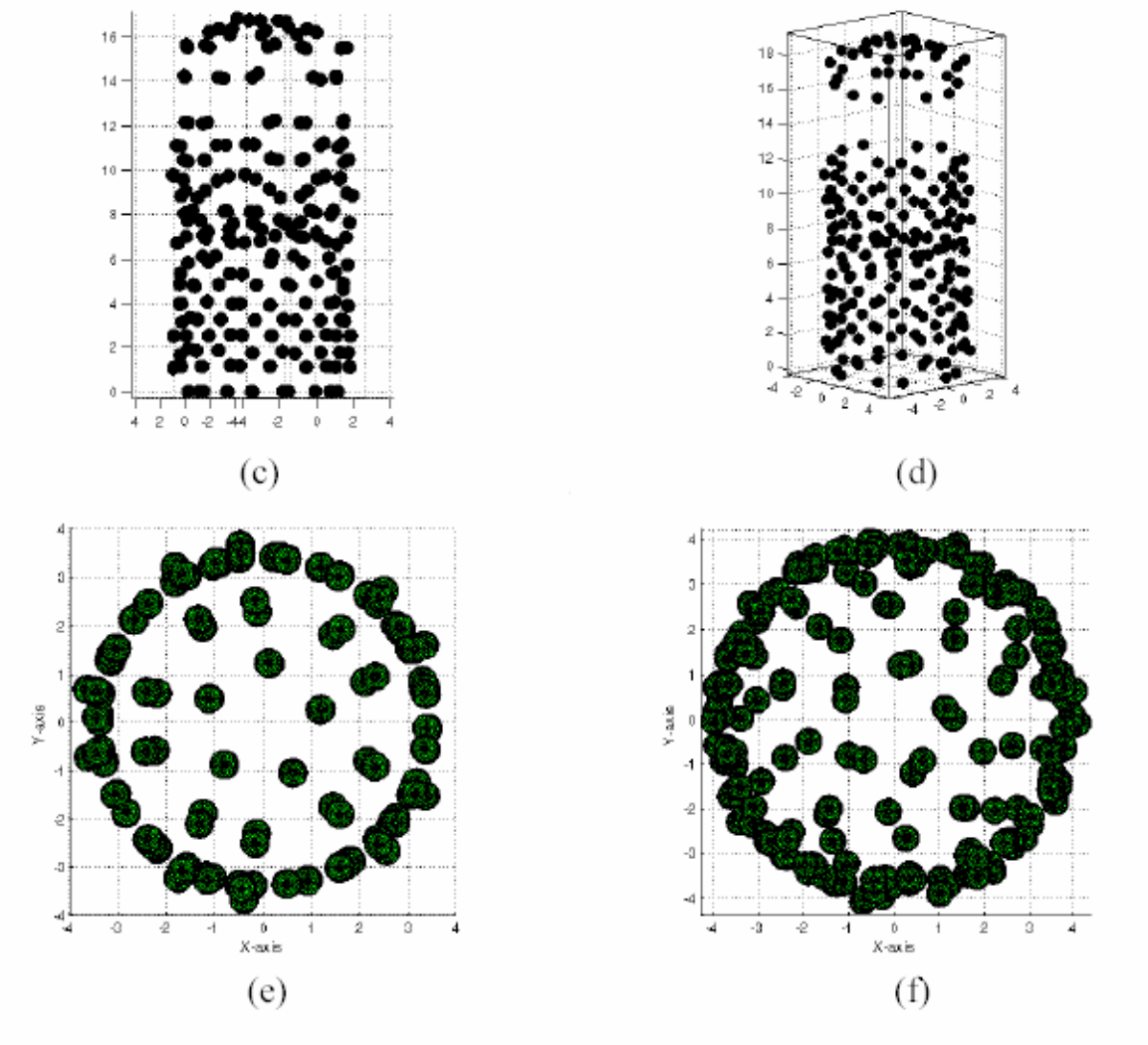

Figure 14. Configurations of BSNT model using non-equilibrium MDSS simulation

Figures 13(b) and 14(b) show the configuration of both models when the applied tensile force is 30 (nN/atom), which means that both models are within the small strain region. Although separation gaps have appeared in both models, their average separation distances are less than the maximum potential influence distance 2 Å between carbon atoms. Beyond the scope of this tensile force, both carbon nanotubes show a characteristic buckling and kicking features at the side tubular wall. These features are also shown in Figure 13(c) and 14(c) when the applied force is 50 (nN/atom).

Figures 13(d) and 14(d) demonstrate that both SWNT and BSNT model separate into two halves (top and bottom) beyond the maximum tensile force (~60 nN/atom),

leading to a fracture which means that the average separation gaps are larger than 2 Å. This separation and fracture are not rapid, but occur gradually due to local interactions or rearrangement between the carbon atoms. However, slip taking place at about 45° to the loading direction, is a general phenomenon in the case of ductile metals, was not be observed explicitly. Rather, under the strong tensile force, they exhibited a brittle material-like feature such as a diamond, which is known as the hardest material consisting of carbon atoms with SP^3 bonding structure. The numerical results for non-equilibrium MDSS simulations for both models will be described in the next section.

Figures 14 (e) and (f) show the changes in the cross-sectional area and distribution of atoms seen from the top view of the BSNT model from the case of initial configuration (e) to the case of large applied tensile force of 75 nN/atom (f). A precise value for the changed cross-sectional area is difficult to obtain, because the amount of distortions of circumferential carbon atoms in the side wall of BSNT model is not obvious. This unclear cross-sectional area during the MDSS simulation will prevent computing the applied stress needed for calculating Young's modulus from MDSS results. Furthermore, it can be found that carbon atoms in the dome-shaped cap region of BSNT model as the applied force increases show the rotational motions on the axis of this BSNT model. Both observations demonstrate that carbon atoms under T-B potential and an external force look for the appropriate position to minimize the system energy. Thus, Figure 14 (f) directly proves that the binding between atoms can be formed or broken due to the induced defects on BSNT model during the non-equilibrium simulation.

D. COMPARATIVE RESULTS OF EQUILIBRIUM AND NON-EQUILIBRIUM MDSS SIMULATIONS

In this section, a relative Young's modulus ratio concept for the SWNT and BSNT will be introduced with the force-strain diagram that is extracted from the non-equilibrium MDSS simulation, which will then be compared with the Young's modulus values calculated from the previous equilibrium MDSS simulation.

By conventional continuum mechanics, the ultimate tensile strength and Young's modulus for a bulk material can be determined from the force-displacement data under the external tensile loading test. The ultimate tensile strength is measured as the maximum stress prior to fracture. To obtain the Young's modulus from the collected data, a second-degree polynomial function can be fitted to the applied force-displacement diagram, with the modulus measured as the slope within the small strain limit range [46].

However, since it is difficult to estimate a definite cross-sectional area of CNTs due to the nano-scale model configuration during the MDSS simulation runs, the above conventional method is not appropriate to calculate a realistic Young's modulus directly from the applied force-strain diagram of non-equilibrium MDSS simulation. For that reason, a relative Young's modulus strength (RYMS) concept, in which two materials are assumed to have the same cross-sectional area, is introduced to remove the effect of cross-sectional area in computing the Young's modulus.

Suppose there are two materials called "1" and "2", with the same cross-sectional area A under a tensile loading test within the elastic strain limit. Then, the Young's modulus of each material "1" and "2" can be calculated by

$$Y_1 = \frac{\sigma_1}{\varepsilon_1}, \quad \text{where } \sigma_1 \text{ and } \varepsilon_1 \text{ is stress and strain of "1" material.} \qquad (39)$$

$$Y_2 = \frac{\sigma_2}{\varepsilon_2}, \quad \text{where } \sigma_2 \text{ and } \varepsilon_2 \text{ is stress and strain of "2" material.} \qquad (40)$$

Since a stress is represented as a force per cross-sectional area F/A, the resultant relative Young's modulus strength (RYMS) for two materials can be rewritten with only applied force and strain as

$$RYMS = \frac{Y_1}{Y_2} = \frac{F_1 \cdot \varepsilon_2}{F_2 \cdot \varepsilon_1} = \frac{F_1}{\varepsilon_1} \cdot \frac{\varepsilon_2}{F_2} \qquad (41)$$

Therefore, the RYMS value can be expressed as the product of forces to strain ratio of material "1" and the reverse of force to strain ratio of material "2". To collect data for the analysis of atomic scale tensile deformations of our SWNT and BSNT models, the tensile forces were applied to both models to move the end atoms with constant strain rates (~10^{-2} /ps), and the strain per atom at every force was measured. Once the force-strain per atom data are collected from the simulation, a relationship between the applied force and strain can be plotted as the force-strain diagram.

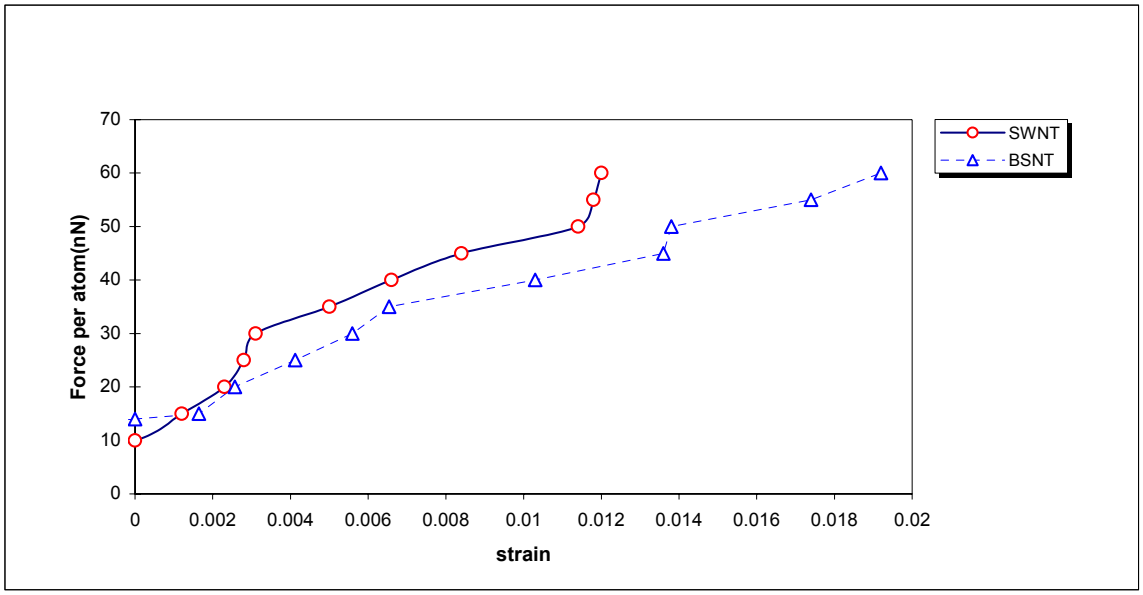

Figure 15. Tensile force-strain per atom for the SWNT and BSNT model.

The tensile force-strain diagram for the SWNT and BSNT obtained from the non-equilibrium MDSS simulation is plotted in Figure 15. The applied tensile forces per atom of the SWNT and BSNT were recorded on the Y-axis, and the average strains of carbon atoms in the location right below the forced atoms were recorded on the X-axis, respectively. On the whole, the observed force-strain diagrams show a significant non-linear relationship. In particular, it is worth to observe that the strain of BSNT is more linearly increased than that of SWNT as the applied force increases. From this observation, it is possible to expect that the Young's modulus of BSNT would be less than the modulus of SWNT.

To calculate the relative Young's modulus strength (RYMS) value between two materials, SWNT and BSWNT, and to satisfy an elastic limit criteria, an applied tensile force range of 15 ~ 30 nN/atom was selected, and the linear regression analysis was applied to this selected data as shown Figure 16. Based on the linear regression analysis under the assumption that there is an elastic limit on a force-strain diagram, the ratio of force to strain of a specific material can be represented as the slope of the regression line.

In Figure 16, though the data set of SWNT shows a more non-linear characteristic than those of BSNT within the same applied force range, the linear regression analysis can be used for both data sets due to a good fitting statistical coefficient R^2, which quantifies a goodness of fit and is a fraction between 0.0 and 1.0, with no units. Higher R^2 values indicate that the fitting line or curve comes closer to the data. In this case, the computed R^2 using the statistical software package was 0.91 for SWNT and 0.99 for BSNT. These numerical values indicate that the linear assumption to calculate the slope of a regression line for SWNT and BSNT is appropriate.

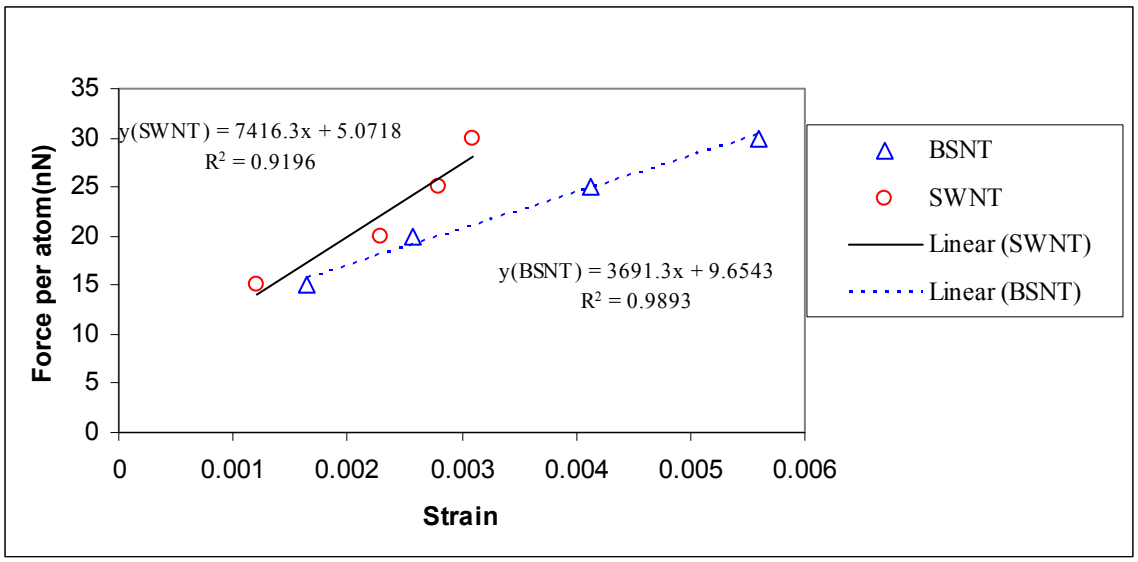

Figure 16. The linear regression fitting for SWNT/BSNT within elastic limit.

The resultant slope of the regression line that is 7416.3 for SWNT and 3691.3 for BSNT can be seen in Figure 16. Consequently, the RYMS value for the BSNT with respect to the SWNT was calculated as 0.498. This means that the average Young's modulus of BSNT model is 49.8 % of that of SWNT. Of course, if the selected range of tensile force is beyond the elastic limit and the linear assumption for the small strain region to find Young's modulus is violated, and then the RYMS value would change significantly.

From the results of the previous equilibrium MDSS simulations, the evaluated mean Young's modulus of SWNT and BSNT were 1.424 TPa and 0.604 TPa, respectively. Based on these two values and equation (41), the calculated RYMS value of the BSNT with respect to SWNT is 0.424 (42.4%). This is consistent with the RYMS value of the non-equilibrium MDSS simulation results, 0.498 (49.8%), within an error of $\pm 15\%$. Consequently, though we could not find an exact numerical value for the Young's modulus of the SWNT and BSNT models from the non-equilibrium MDSS simulations, the Young's modulus of BSNT model was observed to be lower than that of the SWNT model using the RYMS comparative study, that is a heterogeneous CNTs might be found to have a lower Young's modulus than pure CNTs. These results show that even the heterogeneous CNTs will have a higher Young's modulus than other real materials such as hardened steel. The heterogeneous CNTs may be a great potential candidate promising the high strength and ultra light-weight composite materials and nano-scale devices in the near future.

IV. CONCLUSION AND RECOMMENDATIONS

A. CONCLUSION

MDSS simulations employing the thermal vibration method under equilibrium and non-equilibrium conditions at the nanoscale were performed on two carbon nanotubes models, namely, single-walled carbon nanotubes (SWNT) and bamboo structural single-walled carbon nanotubes (BSNT) that represents a heterogeneous CNTs. For the many-body empirical potential, the Tersoff-Brenner potential was used to evaluate the Young's modulus and mechanical behavior of SWNT and BSNT.

The measured mean Young's moduli of the SWNT and BSNT models were 1.424 TPa and 0.604 TPa, respectively. In particular, the calculated Young's modulus of the SWNT model using the MDSS code and the freestanding thermal vibration method presented by Krishnan *et al.* were in reasonable agreement with results reported in the literature based on various theoretical calculations and nano-scale experimental studies as shown Table 3 and 4.

Furthermore, even though the evaluated Young's modulus of BSNT, which has an internal support structure and was assumed to be a hetero-junction nanotube consisting of two armchair (5, 5) SWNTs with the same diameter, was significantly less than the pure armchair (5, 5) SWNT Young's modulus due to the induced defects such as pentagon and heptagon type rings at the junction region of the two SWNTs, however it still has strong and stiff mechanical characteristics along the axis of the tube than other general bulk materials such as hardened steel. It holds a promising future for the variety of potential applications in the nanotechnology field.

B. RECOMMENDATIONS

The calculational technique developed in this thesis was numerically efficient in computing the mechanical characteristics of SWNT and BSNT type models, and would be useful tool for design and analysis of composite materials at the atomic or molecular

level. Therefore, there will be various and numerous real applications for this developed computational technique. It is strongly recommended that further study be conducted in the following areas:

1. Other dynamic or static mechanical properties of the SWNT/BSNT models can be investigated such as bending stiffness, torsion stiffness or shear modulus under a wide variety of loading cases and different realistic thermodynamic ensembles such as the Langevin friction force scheme to control the kinetic temperature and simulation time step [47].

2. Quantitative and qualitative analysis for the formation energy aspects of diverse defects such as pentagon or heptagon ring defects in CNTs should be researched to test whether it significantly affects the mechanical and electronical properties of carbon nanotubes.

3. By applying quantum mechanics with more accurate and realistic inter-atomic potential functions to CNTs, the nano-electronic characteristics of CNTs such as an armchair-armchair or armchair-zigzag hetero-junctions may be known by investigating the metallic and semiconducting behaviors as well as the electronic transport properties.

4. It is strongly recommended to develop new potential functions that would be used to simulate interactions between carbon nanotubes and other materials in the embedded nanotube polymer composite materials, with the designed models for real applications such as body armor or embedded nano-devices it may be simulated and tested whether it will be efficient and applicable or not.

LIST OF REFERENCES

[1] S. Iijima, 1991: Helical microtubles of graphitic carbon. *Nature*., **354**, 56-58.

[2] J. D. H. Hughes, 1987: The evaluation of current carbon fibers. *J. Phys*., **D 20**, 276-285.

[3] M. S. Dresselhaus, and M. Endo, cited 2003: Relation of Carbon Nanotubes to other Carbon Materials. [http://www.ce.udel.edu/~baidurya/downloads/Topics/20matls.pdf]

[4] M. F. Yu, O. Lourie, M. J. Dyer, K. Moloni, T. F. Kelly, and R. S. Ruoff, 2000: Strength and breaking mechanism of multiwalled carbon nanotube under tensile load. *Science*, Vol. **287**, 637-640.

[5] O. L. Blakslee, D. G. Proctor, E. J. Seldin, G. B. Spence, and T. Weng, 1970: Elastic constants of Compression-Annealed Pyrolytic Graphite. *J. Appl. Phys*. **41**, 3373-3389.

[6] S. O. Kasap, 2002: *Principles of Electronic Materials and Devices*, McGraw-Hill, New York, 745 pp.

[7] G. Overney, W. Zhong, and D. Tománek, 1993: Structural Rigidity and Low Frequency Vibrational Modes of Long Carbon Tubules, *Z. Phys*. D **27**, 93-96.

[8] D. H. Robertson, D. W. Brenner, and J. W. Mintmire, 1992: Energetics of Nanoscale Graphite Tubules. *Phys. Rev*. **B 45**, 12592-12595..

[9] B. I. Yakobson, C. J. Brabec, and J. Bernholc, 1996: Nanomechanics of Carbon Tubes: Instabilities beyond linear response. *Phys. Rev. Lett*. **76**, 2511-2514.

[10] M. Menon and D. Srivastava, 1997: Carbon Nanotube "T Junctions": Nanoscale Metal-Semiconductor-Metal Contact Devices. *Phys. Rev. Lett*. 79, 4453–4456.

[11] T. Rueckes, K. Kim, E. Joselevich, G. Y. Tseng, C-L Cheung, and C. M. Lieber, 2000: Carbon Nanotube-Based Nonvolatile Random Access Memory for Molecular Computing. *Science*. **289**, 94-97.

[12] A. N. Andriotis, M. Menon, D. Srivastva, and L. Chernozatonskii, 2002: Transport Properties of single-wall carbon nanotube Y junctions. *Phys. Rev. B.* **65**, 165416 (1-13).

[13] Iljin Nanotech. R & D center, cited 2 April 2003: Structural characteristics of CNT. [http: www.iljinnanotech.co.kr/ kr/ home.html]

[14] D. Srivastava, Chenyu Wei, and Kyeongjae Cho, 2003: Nanomechanics of carbon nanotubes and composites. *Appl. Mech. Rev*. **56**, no 2, 215-230.

[15] M. Meyyappan, and D. Srivastava, 2000: Carbon Nanotubes. *NASA Ames Research Center*, 55 pp.

[16] A. Krishnan, E. Dujardin, T. W. Ebbesen, P. N. Yianilos and M. M. J. Treacy, 1998: Young's modulus of single-walled nanotubes. *Phys. Rev. B*. **58**, 14013-14019.

[17] C. Schonenberger, cited 19 Novemer 2003: Carbon Nanotubes. [http: www.physicsweb.org/article/world/11/ 1/ 9]

[18] M. S. Dresselhaus, G. Dresselhaus and P. C. Eklund, 1996: *Science of Fullerenes and Carbon Nanotubes*, Academic Press, New York, 965 pp.

[19] C. Schönenberger, A. Bachtold, C. Strunk, J.-P. Salvetat and L. Forró, 1999: Interference and interaction in multiwall carbon nanotubes. *Appl. Phys. A*. **69**, 283-295.

[20] D. H. Oh, and Young Hee Lee, 1998: Stability and cap formation mechanism of single-walled carbon nanotubes. *Phy. Rev. B*. **58**, 7407-7411.

[21] T. Rueckes, K. Kim, E. Joselevich, G. Y. Tseng, C-L Cheung, and C. M. Liever, 2000: Carbon Nanotube-Based Nonvolatile Random Access Memory for Molecular Computing. Science. 289, 94-97.

[22] A. Zettl, and John Cumings, 2000: Low-Friction Nanoscale Linear Bearing Realized from Multiwall Carbon Nanotubes. *Science*. **289**, 602-604.

[23] N. J. Giordano, 1997: *Computational Physics*, Prentice Hall, New Jersey, pp. 232 - 252.

[24] L. N. Hand, and J. D. Finch, 1998: *Analytical Mechanics*, Cambridge University Press, New York, pp. 175 – 184.

[25] J. M. Haile, 1997: *Molecular Dynamics Simulation: Elementary Methods*, John Wiley & Sons, Inc., New York, pp. 438 - 461.

[26] G. C. Abell, 1984: Empirical chemical pseudopotential theory of molecular and metallic bonding. *Phys. Rev. B*. **31**, 6184-6196.

[27] J. Tersoff, 1987: New empirical approach for the structure and energy of covalent systems. *Phys. Rev. B*. **37**, 6991-7000.

[28] D. W. Brenner, 1990: Empirical potential for hydrocarbons for use in simulating the chemical vapor deposition of diamond films. *Phys. Rev. B*. **42**, 9458-9471.

[29] W. G. Wilder, L. C. Venema, A. G. Rinzler, R. E. Smalley, and C. Dekker, Nature **391**, 6662 (1998).

[30] T. W. Odom, Jin-Lin Huang, Philip Kim, and C. M. Lieber, Nature **391**, 6662 (1998).

[31] Stephen T. Thornton and Andrew Rex, 2000: *Modern Physics for Scientists and Engineers*, Sanders College Publishing. Inc, Orlando, pp. 202-207.

[32] S. O. Kasap, 2002: *Principles of Electronic Materials and Devices*, McGraw-Hill, New York, pp. 27-30.

[33] S. O. Kasap, 2002: *Principles of Electronic Materials and Devices*, McGraw-Hill, New York, pp. 18-21.

[34] J. M. Haile, 1997: *Molecular Dynamics Simulation: Elementary Methods*, John Wiley & Sons, Inc., New York, pp. 157 - 177.

[35] M. H. Kalos, 1984: *Monte Carlo Methods in Quantum Problems*, NATO ASI Series C, Vol. 125, Reidel, Dordrecht , Holland.

[36] M. K. Pelosi, T. M. Sandiffr, and U. Sekaran, 2001: *Research and Evaluation for Business*, John Wiley & Sons, Inc. pp. 290-310.

[37] B. I. Yakobson, C. J. Brabec, and J. Bernholc, 1996: Nanomechanics of Carbon Tubes: Instabilities beyond Linear Response. *Phys. Rev. Lett*. **76**, 2511-2514.

[38] J. P. Lu, 1997: Elastic properties of carbon nanotubes and nanoropes, *Phys. Rev. Lett*, **79**, 1297-1300.

[39] E. Hernandez, C. Goze, P. Bernier, and A. Rubio, 1998: Elastic Properties of C and $B_xC_yN_z$ Composite Nanotubes. *Phys. Rev. Lett*. **80**, 4502-4505.

[40] D. Sanchez-Portal, E. Artacho, J. M. Solar, A. Rubio, and P. Ordejon, 1999: *Ab initio* structural, elastic, and vibrational properties of carbon nanotubes. *Phys. Rev. B.* **59**, 12678-12688.

[41] P. Poncharal, Z. L. Wang, D. Ugarte, and W. A. DeHeer, 1999: Electrostatic deflections and electromechanical resonances of carbon nanotubes, *Science***.** **283**, 1513-1516.

[42] S. Iijima, C. J. Brabec, A. Maiti, and J. Bernholc, 1996*:* Structural flexibility of Carbon Nanotubes, *J. Chem. Phys*. **104**, 2089-2092.

[43] A. Krishnan, E. Dujardin, T. W. Ebbesen, P. N. Yianilos and M. M. J. Treacy, 1998: Young's modulus of single-walled nanotubes. *Phys. Rev. B*. **58**, 14013-14019.

[44] E.W. Wong, P.E. Sheehan, and C.M. Lieber, 1997: Nanobeam mechanics : Elasticity, strength, and toughness of nanorods and nanotubes, *Science*. **277**, 1971-1975.

[45] A. Higdon, E. H. Ohlsen, W. B. Stiles, J. A. Weese, and W. F. Riley, 1985: *Mechanics of Materials; Fourth Edition*, John Wiley & Sons, Inc., New York, pp. 744

[46] P. Heino, H. Häkkinen, and K. Kaski, 1998: Molecular dynamics study of copper with defects under strain. *Phys. Rev. B*. **58**, 641-652.

[47] J. C. Tulley, Y. J. Chabal, K. Raghavachari, J. M. Bowman, and R. R. Lucchese, 1985 : Infrared linewidths and vibrational lifetimes at surfaces: H on Si (100). *Phys. Rev. B*. **31**, 1184-1186.

THIS PAGE INTENTIONALLY LEFT BLANK

INITIAL DISTRIBUTION LIST

1. Defense Technical Information Center
   Ft. Belvoir, Virginia

2. Dudley Knox Library
   Naval Postgraduate School
   Monterey, California

3. Professor & Chair Young W. Kwon
   Department of Mechanical Engineering and Energy Processes
   Southern Illinois University
   Carbondale, Illinois

4. James H. Luscombe
   Naval Postgraduate School
   Monterey, California

5. James V. Sanders
   Naval Postgraduate School
   Monterey, California

6. Engineering & Technology Curricular Office (Code 34)
   Naval Postgraduate School
   Monterey, California

7. Major Oh, Jung Joo, ROK Army
   243 (8 tong 4 ban) Gu-Hwang dong,
   Kyoung-ju, Kyoungbook, Republic of Korea